Journal of Molecular Catalysis A: Chemical 346 (2011) 55–69

Contents lists available at ScienceDirect

Journal of Molecular Catalysis A: Chemical

journal homepage: www.elsevier.com/locate/molcata

Chain growth mechanism of Fischer–Tropsch synthesis on $Fe_5C_2(0\,0\,1)$

Dong-Bo Cao[a], Yong-Wang Li[a], Jianguo Wang[a], Haijun Jiao[a,b,*]

[a] State Key Laboratory of Coal Conversion, Institute of Coal Chemistry, Chinese Academy of Sciences, Taiyuan 030001, PR China
[b] Leibniz-Institut für Katalyse e.V. an der Universität Rostock, Albert-Einstein-Strasse 29a, 18059 Rostock, Germany

ARTICLE INFO

Article history:
Received 12 January 2011
Received in revised form 17 June 2011
Accepted 21 June 2011
Available online 28 June 2011

Keywords:
FTS
$Fe_5C_2(0\,0\,1)$
DFT
Insertion mechanism
Carbide mechanism

ABSTRACT

The chain growth mechanisms of Fischer–Tropsch synthesis on $Fe_5C_2(0\,0\,1)$ were investigated at the levels of density functional theory. On the H_2 and CO co-adsorbed surface, the formation of CH and CCO is the most favored initial steps. The subsequent steps of CCO coupling with C into CCCO and CCO hydrogenation into CCH_2 and CHCH are competitive. Furthermore, CCH from CCH_2 and CHCH dehydrogenation can couple with C to form CCCH. Since chain initiation from CO insertion obeys insertion mechanism, and chain propagation from CCH coupling obeys carbide mechanism, both mechanisms are operative and co-operative in Fischer–Tropsch synthesis. The carburized active surfaces can be regenerated and maintained by CO adsorption on the vacancy site, followed by hydrogenation into surface formyl (CHO) and successive dissociation into surface CH and O. In addition surface O can be hydrogenated into surface OH, and H_2O formation from surface OH disproponation is energetically more favored than surface OH hydrogenation.

1. Introduction

Iron-based catalysts are widely used in industrial Fischer–Tropsch synthesis (FTS) [1], which becomes increasingly important especially for liquid fuel production under the background of the predicted lack of crude oil supply. In FTS, iron carbides are the active phases of iron-based catalysts [2–9] and the Hägg iron carbide (Fe_5C_2) is the most representative one. Transmission electron microscopy, Mössbauer spectroscopy and X-ray analysis reveal the responsibility of the highly dispersed Fe_5C_2 for the high FTS activity [3–7]. FTS products are rather complex, including linear paraffins, α-olefins and a small amount of oxygenated compounds such as alcohols, aldehydes, ketones, acids, as well as H_2O and CO_2 [10–12]. Both experimental and theoretical studies have been dedicated to FTS mechanisms, and some insights are outlined below.

Carbide mechanism, originally proposed by Fischer and Tropsch [13], was put forward by Pettit et al. and Biloen et al. [14–17]. They proposed the formation pathway of surface CH_2 and alkyl polymerization scheme. However, the critical point of carbide mechanism is chain initiation, which remains serious debates. Mims et al. [18] used isotopic transient experiment to study high hydrocarbon formation on Ru catalysts, and suggested vinylidene (CH_2C) or ethylidene (CH_3CH) as possible C_2 initiator. Turner [19–25] and Jordan et al., [26,27] showed that C_2 species, derived from either vinyl-X (X = Br, SiR_3, etc.) or ethane probes, are incorporated into hydrocarbons over a number of metals, and vinyl (CH_2CH) is involved in initiating polymerization in many experiments [28–32]. Ciobîcă et al. [33,34] studied the FTS mechanism on Ru(0 0 0 1) using dynamic Monte Carlo and density functional theory (DFT) method, and found CH as the most likely monomer, as well as $CHCH_2$ and $CHCH_3$ as C_2 initiators. On the basis, they [35] proposed the parallel mechanisms of alkylidene (methylene-like) and alkyl (methyl-like) intermediates. Liu et al. [36,37] studied all possible C–C coupling reactions on flat and stepped Ru(0 0 0 1) and stepped Rh(1 1 1) using DFT method, and found C + CH as the most favored reaction on stepped Ru(0 0 0 1) and Rh(1 1 1). Lo and Ziegler [38] studied chain initiation on Fe(1 0 0) with DFT method, and found $C + CH_2$ as the most likely reaction pathway and $C + (CCCH_2/CCCH_3)$ as the most favored pathway for chain propagation [39]. On the $Fe_3C(1\,0\,0)$ surface, Deng et al. found that surface C_2H_x formation comes from CO insertion into surface carbon followed by C–O bond dissociation and hydrogenation [40]. Although carbide mechanism can explicitly explain the formation of hydrocarbons, it cannot explain the formation of oxygenated products [41].

CO insertion mechanism was proposed by Pichler and Schulz [42], in which C + C coupling via CO insertion into adsorbed alkyl with the formation of surface acyl (RCO–) may result in alkyl, alkenes and oxygenates. Emmett et al. [43,44] added radioactive alcohol, ethylene, propionaldehyde and propanol etc. into syngas ($CO + H_2$), and found the C_2–C_{10} products containing radioactive carbon atom, suggesting primary alcohols added as starting nuclei in building up higher hydrocarbons. For CO hydrogenation, the barrier of CHO hydrogenation is 0.45 eV lower than that of dissociation on flat Co(0 0 0 1) [45,46]. On flat and stepped Co(0 0 0 1), the barrier

* Corresponding author at: Leibniz-Institut für Katalyse e.V. an der Universität Rostock, Albert-Einstein-Strasse 29a, 18059 Rostock, Germany.
Tel.: +49 381 1281 135; fax: +49 381 1281 5000.
E-mail address: haijun.jiao@catalysis.de (H. Jiao).

1381-1169/$ – see front matter © 2011 Elsevier B.V. All rights reserved.
doi:10.1016/j.molcata.2011.06.009

of CH_2O hydrogenation is 0.09 and 0.40 eV lower than that of dissociation, respectively [45], and the favored product is CH_3OH instead of CH_x. However, the products of ketene (CH_2CO) hydrogenation on Fe_5C_2(0 0 1) are hydrocarbon instead of ethanol [47]. Therefore, the CO insertion mechanism leading either to oxygenates or to hydrocarbons needs to be understood in detail.

Anderson [48] and Eidus [49] proposed hydroxycarbene mechanism, in which the condensation of two M=CHOH group results in CHCOH formation, which can be further hydrogenated to hydrocarbons and oxygenates. Hydroxycarbenes as ligands have been found in transition metal complexes, such as $(CO)_5Cr{=}C(OH)Ph$ [50] and $(CO)_2Re{=}C(OH)CH_2CH_2(\eta^5\text{-}C_5H_4)$ [51].

Apart from hydrocarbons, H_2O also is a primary product from FTS [52]. It is believed that high H_2O concentration is one factor for oxidation and deactivation of iron carbides [53–56], and therefore understanding H_2O formation and desorption is important for enhancing FTS activity. Michaelides and Hu [57,58] used DFT methods to investigate the microscopic reactions of H_2O formation on Pt(1 1 1), and reported the detailed mechanism. Gong et al. [59] performed DFT calculations to study the mechanism of H_2O formation on flat and stepped Co(0 0 0 1) surfaces, and found the H_2O formation is favored at high coverage.

In our theoretical study on chain growth mechanism, both carbide and CO insertion mechanisms on Fe_5C_2(0 0 1) are considered. Under a wide range of conditions, there are many different intermediates, which may lead to the same products from different pathways. We investigated all possible $C_1 + C_1$ couplings for C_2 initiator. On the basis of the favored C_2 formation, the chain growth through $C_2 + C_1$ coupling was studied. Furthermore, chain growth mechanism on Fe_5C_2(0 0 1) was discussed, and compared with chain initiation mechanism on other Fe_xC surfaces. In addition, the mechanism of H_2O formation on Fe_5C_2(0 0 1) was studied.

2. Methods and models

All calculations were performed at the DFT level using the Cambridge sequential total energy package (CASTEP) [60,61]. Ionic cores were described by ultrasoft pseudopotential [62] and PBE functional [63] (USPP–PBE) and the Kohn–Sham one-electron states were expanded in a plane wave basis set up to 340 eV. A Fermi smearing of 0.1 eV was utilized. Brillouin zone integration was approximated by a sum over special *k*-points chosen using the Monkhorst–Pack scheme [64]. The pseudopotential with partial core was used in spin-polarized calculations to include non-linear core corrections [65]. Spin polarization was used to calculate the energies and structures of isolated C_xH_y and C_xH_yO. Without counting the adsorbate, the vacuum of the slabs was set to span a range of 10 Å to ensure no significant interaction between the slabs. The convergence criteria for structure optimization and energy calculation were set to: (a) SCF of 2.0×10^{-6} eV/atom; (b) energy of 2.0×10^{-5} eV/atom; (c) displacement of 2.0×10^{-3} Å; (d) force of 0.05 eV/Å (0.25 eV/Å for transition state structure calculation).

The transition state structures were located by using the complete LST/QST [66] method in CASTEP. It starts with linear synchronous transit (LST) maximization, followed by energy minimization in directions conjugate to the reaction pathway. The approximated TS is further used to perform quadratic synchronous transit (QST) maximization. From that point, another conjugate gradient minimization is performed. The cycle is repeated until a stationary point is located. We also calculated the transition state structures of $C_1 + C_1$ coupling reactions using the VASP–PAW–PBE method with the convergence criteria for structure optimization and energy calculation: (a) SCF of 1.0×10^{-4} eV; (b) energy of 1×10^{-3} eV; and (c) force of 0.05 eV/Å. Reasonable agreements between VASP–PAW–PBE and CASTEP–USPP–PBE have been found (Supporting Information). Reasonable agreements between VASP and CASTEP also have been found for CH_x hydrogenations on Fe_5C_2(0 0 1) [67], and ethene epoxidation on two oxidized Ag(1 1 1) surfaces [68].

The vibrational frequencies of adsorbed species and transition state structures were calculated with VASP. This was done with the frozen phonon mode approximation in which the metal atoms are fixed at the relaxed geometries. Due to the large mass difference between Fe and surface carbon species, the vibrations of Fe atoms can be neglected. The Hessian matrix was determined based on a finite difference approach with a step size of 0.02 Å for the displacements of the individual atoms of the adsorbates along each Cartesian coordinate. By diagonalizing the mass-weighted Hessian matrix, the corresponding frequencies and normal modes have been determined. The optimized structures are true energy minimum states with only real frequencies. The optimized transition structures have only one imaginary frequency.

As shown in the side view of Fe_5C_2(0 0 1) in Fig. 1, in order to compare with carbon hydrogenation [67], we used a model system

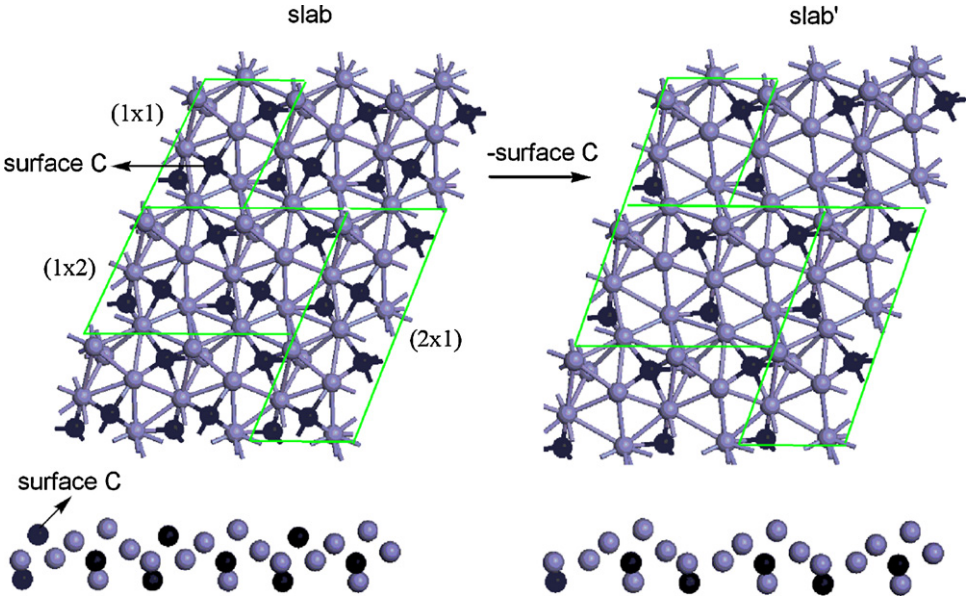

Fig. 1. Top and side views of the Fe_5C_2(0 0 1) slab.

Table 1
Computed activation energy and reaction energy (eV) of CH_xO hydrogenation and C–O cleavage of CH_xO species on $Fe_5C_2(0\,0\,1)$.

	ΔE[a]	$E_{a(f)}$[b]	$E_{a(r)}$[c]	$\Delta H_{(c)}$[d]
$CO \rightarrow C + O$ (**1a**)	0.11	2.98	2.66	0.32
$CO + H \rightarrow HCO$ (**1b**)	0.00	1.39	0.41	0.98
$CHO \rightarrow CH + O$ (**2a**)	0.46	1.16	1.21	−0.05
$CHO + H \rightarrow CH_2O$ (**2b**)	0.00	0.91	0.45	0.46
$CH_2O \rightarrow CH_2 + O$ (**3a**)	0.24	0.69	0.78	−0.09
$CH_2O + H \rightarrow CH_3O$ (**3b**)	0.00	1.06	0.62	0.44
$C + CO \rightarrow CCO$ (**4a**)	0.00	0.66	0.65	0.01
$C + H \rightarrow CH$ (**4b**)	0.00	0.52	0.67	−0.15
$CH + CO \rightarrow CHCO$ (**4c**)	0.00	1.04	0.32	0.72
$CH + H \rightarrow CH_2$ (**4d**)	0.06	0.79	0.02	0.77
$CH_2 + H \rightarrow CH_3$ (**4e**)	0.02	0.51	0.69	−0.18
$CH_3 + H \rightarrow CH_4$ (**4f**)	0.26	0.95	0.75	0.20

[a] For a reaction ($A + B \rightarrow AB$), $\Delta E = [E(A + B/slab) + E(slab)] - (E(A/slab) + E(B/slab))$ for co-adsorbed A and B.
[b] $E_{a(f)} = [E(TS) + E(slab)] - (E((A + B)/slab)$ for the forward energy barrier.
[c] $E_{a(r)} = [E(TS) + E(slab)] - (E(AB/slab)$ for the reversed energy barrier.
[d] $\Delta H_{(c)} = E(AB/slab) - E((A + B)/slab)$ for reaction energy.

with five iron layers and three carbon layers (5Fe/3C), in which the bottom two iron layers and two carbon layers (2Fe/2C) are fixed in their bulk positions, while the three iron layers and one carbon layer on the top (3Fe/1C) can relax. The top layer of $Fe_5C_2(0\,0\,1)$ has both Fe and C in 1:1 ratio, while the second and third layers contain only Fe atoms. A model system with eight iron layers and three carbon layers (8Fe/3C) under the relaxation of the top five iron layers and two carbon layers (5Fe/2C) was tested, and the differences in energy barrier and reaction energy of $C + CH \rightarrow CCH$ and $C + CH_3 \rightarrow CCH_3$ reactions are 0.07 vs. 0.10, and 0.09 eV vs. 0.07 eV, respectively, which validate the applicability of our model. A $3 \times 5 \times 2$ *k*-grid sampling within the Brillouin zones was used in the $p(1 \times 1)$ unit cell. $3 \times 2 \times 2$ and $2 \times 5 \times 2$ *k*-grid samplings within the Brillouin zones were used in the $p(1 \times 2)$ and $p(2 \times 1)$ unit cells, respectively. Since the top layer of $Fe_5C_2(0\,0\,1)$ has carbon atoms, and Stockwell et al. [69] verified with ^{13}C traces that surface carbons of carbide catalysts are incorporated in the FTS products, surface carbon coupling with CH_x and CO also was studied.

For the C_2 and C_3 surface adsorbates, the adsorption energy is defined as $\Delta E_{ads} = (1/n)[E(n\text{-absorbate/slab}') - E(\text{slab}')] - E(\text{absorbate})$, where $E(\text{absorbate/slab}')$ is the total energy for the slabs excluding surface carbon atom with adsorbate formed on the surface, $E(\text{slab}')$ is the total energy of the slab excluding surface carbon atom, $E(\text{absorbate})$ is the total energies of free absorbate and n is the number of adsorbate.

For coupling reaction like A + B = AB, the reaction energy is given under two definitions: (a) $\Delta H_{(s)} = [E(AB/slab) + E(slab)] - [E(A/slab) + E(B/slab)]$, where $E(A/slab)$, $E(B/slab)$ and $E(AB/slab)$ are the total energies for the separately adsorbed A/slab, B/slab and AB/slab, respectively. $\Delta H_{(s)}$ was deduced from the most stable states of the reactants and products for getting the thermodynamics without lateral interaction among the adsorbates (negligible coverage effect). (b) $\Delta H_{(c)} = E(AB/slab) - E((A + B)/slab)$; where $E((A + B)/slab)$ is the total energy of the co-adsorbed (A + B)/slab, and $\Delta H_{(c)}$ reflects the thermodynamics at a defined coverage and includes the effect of lateral interactions. The energy barrier without lateral interaction between reactant and transition state is defined as: $E_a = [E(TS) + E(slab)] - (E((A + B)/slab)$. The lateral interaction of A and B in the co-adsorbed state is the difference between $\Delta H_{(s)}$ and $\Delta H_{(c)}$.

We also have investigated zero-point energy (ZPE) correction with VASP on the reaction energies and the activation barriers. We found that ZPE correction has only a slight effect (about 0.1 eV) on the calculated energies (energies without ZPE correction were shown in Supporting Information).

The reaction rate (r_i) of some reactions (both forward and back) is calculated using the harmonic transition state theory; $r_i = A \exp(-E_a/RT)\theta_A\theta_B$, where A is the pre-exponential factor [70], which may be assumed to be $10^{13}s^{-1}$, and E_a is the activation barrier. Since the reaction temperature of FTS is at 483–543 °C [71]; the rate constants (forward and back reactions) at 483 K and 543 K are calculated. For all reactions, rate constants increase by a factor of 10–100 from 483 K to 543 K.

3. Results and discussion

After CO and H_2 co-adsorption, surface CO, H and C are formed; and surface C hydrogenation, CO dissociation and hydrogenation, as well as CO coupling with CH_x are possible. We previously computed surface C hydrogenation on $Fe_5C_2(0\,0\,1)$, and found that surface CH should be the most favorable species, and the last step to form CH_4 has the highest barrier [67]. For comparison, CO dissociation and hydrogenation as well as coupling with surface CH_x are further studied.

3.1. CO dissociation, hydrogenation and coupling

For CO dissociation and hydrogenation, the computed reaction barriers and energies are shown in Table 1. The potential energy surface (PES) of CO hydrogenation and dissociation is shown in Fig. 2, and the transition state structures are shown in Fig. 3.

The lateral interaction of co-adsorbed C, CH, CH_2, and O atom is 0.11, 0.46, and 0.24 eV, respectively. There are no lateral interaction of co-adsorbed CO, CHO, CH_2O and H atom. The barrier of CO dissociation ($CO \rightarrow C + O$, **1a**) and hydrogenation ($CO + H \rightarrow CHO$, **1b**) is 2.98 and 1.39 eV, respectively, and **1b** is preferred kinetically, but both reactions are endothermic (0.32 eV vs. 0.98 eV). As the second step, the barrier of CHO dissociation ($CHO \rightarrow HC + O$, **2a**) and hydrogenation ($CHO + H \rightarrow CH_2O$, **2b**) is 1.16 and 0.91 eV, respectively, and **2b** is preferred kinetically, while **2a** is favored thermodynamically (−0.05 eV). As the third step, the barrier of CH_2O dissociation ($CH_2O \rightarrow CH_2 + O$, **3a**) and hydrogenation ($CH_2O \rightarrow CH_3O$, **3b**) is 0.69 and 1.06 eV, respectively, and **3a** is preferred kinetically and thermodynamically (−0.09 eV). While $CH_2 \rightarrow CH + H$ is favored both kinetically (0.02 eV) and thermodynamically (−0.77 eV), CO hydrogenation prefers to form CH rather than CH_3OH on $Fe_5C_2(0\,0\,1)$. This differs from CO hydrogenation on flat and stepped Co(0 0 0 1) [45], where the barrier of CH_2O hydrogenation is 0.09 and 0.40 eV lower than that of CH_2O dissociation, respectively, and the favored product is CH_3OH instead of CH_2.

To compare surface C hydrogenation, the reaction barriers of CH_x hydrogenation on $Fe_5C_2(0\,0\,1)$ studied previously [67] are included in Table 1. The PES of C hydrogenation is also shown in Fig. 2. Surface C hydrogenation has barrier of 0.52 eV, and is exothermic by 0.15 eV, the barrier of CO hydrogenation of 1.39 eV

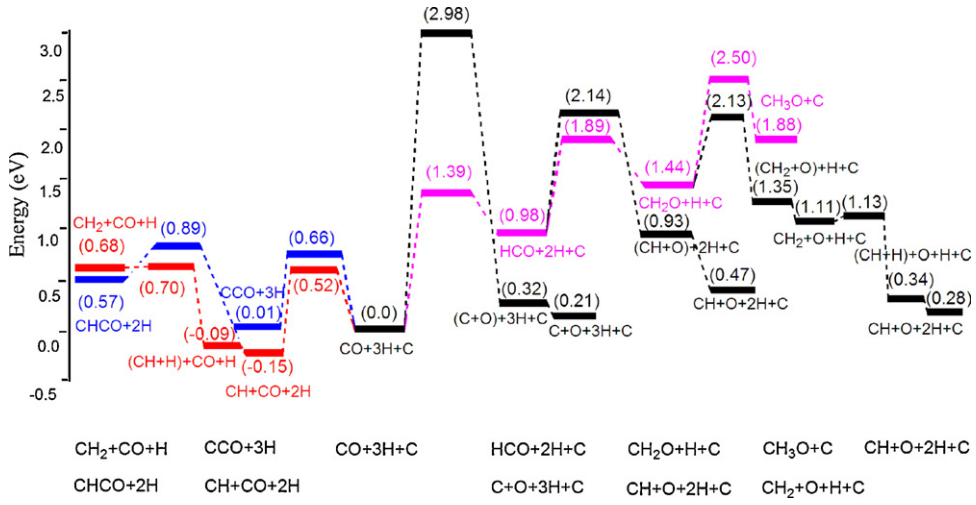

Fig. 2. Potential energy surface of CO hydrogenation (pink line), dissociation (black line), and coupling reaction (blue line), and C hydrogenation (red line) on $Fe_5C_2(0\,0\,1)$. (For interpretation of the references to colour in this figure legend, the reader is referred to the web version of this article.)

is much higher. Therefore, surface C hydrogenation to form CH is more favorable than CO hydrogenation to form CHO. From the above comparison, surface CH is the most populated species, from either CO hydrogenation way or C hydrogenation way.

For CO coupling with C and CH, the reaction barriers and energies also are listed in Table 1, and the transition state structures of $CH_x + CO$ couplings are shown in Fig. 3. Since surface CH_2 dissociates easily into CH, the reactions of $CH_2 + CO$ and $CH_3 + CO$ are shown in Supporting Information. Other $CH_x + CH_x$ coupling reactions also are shown in Supporting Information.

No lateral interaction between C with CO and H atom is found. The reaction of CO + C has barrier of 0.66 eV, and is slightly endothermic by 0.01 eV. The comparable barriers (0.66 and 0.52 eV) of C + CO (**4a**) and C + H (**4b**) show that both reactions are favored kinetically. However, **4b** is more favored thermodynamically than **4a** on the basis of the reaction energies (−0.15 eV vs. 0.01 eV). In addition, CH + CO coupling (**4c**) has barrier of 1.04 eV and is endothermic by 0.72 eV, and its back reactions is much favorable. No lateral interaction of co-adsorbed CH and CO is found. Therefore, CH and CCO are the main surface species along with CO and H on $Fe_5C_2(0\,0\,1)$ for the first step of FTS reactions.

3.2. CCO hydrogenation, dissociation and coupling

Along with CCO coupling with CH/CO, the competitive CCO hydrogenation to CHCO/CCHO, and dissociation into C_2 and O are included for comparison. The computed reaction barriers and energies are listed in Table 2. The PES of CCO coupling is shown in Fig. 4, and the transition state structures of CCO coupling are shown in Fig. 5. The PES of CCO hydrogenation and dissociation is shown in Fig. 6, and the transition state structures are shown in Fig. 7.

As shown in Table 2, the lateral interaction between CCO and CO, CH is 0.11 and 0.13 eV, respectively. CCO + CO (**5a**) and CCO + CH (**5b**) couplings have high barriers (1.43 eV vs. 1.71 eV), and they also are endothermic (0.49 eV vs. 0.05 eV), and these barriers are higher that that of CH dehydrogenation (0.67 eV, back reaction of **4b**). In the transition state structures of CCO + CH (**5a**) and CCO + CO

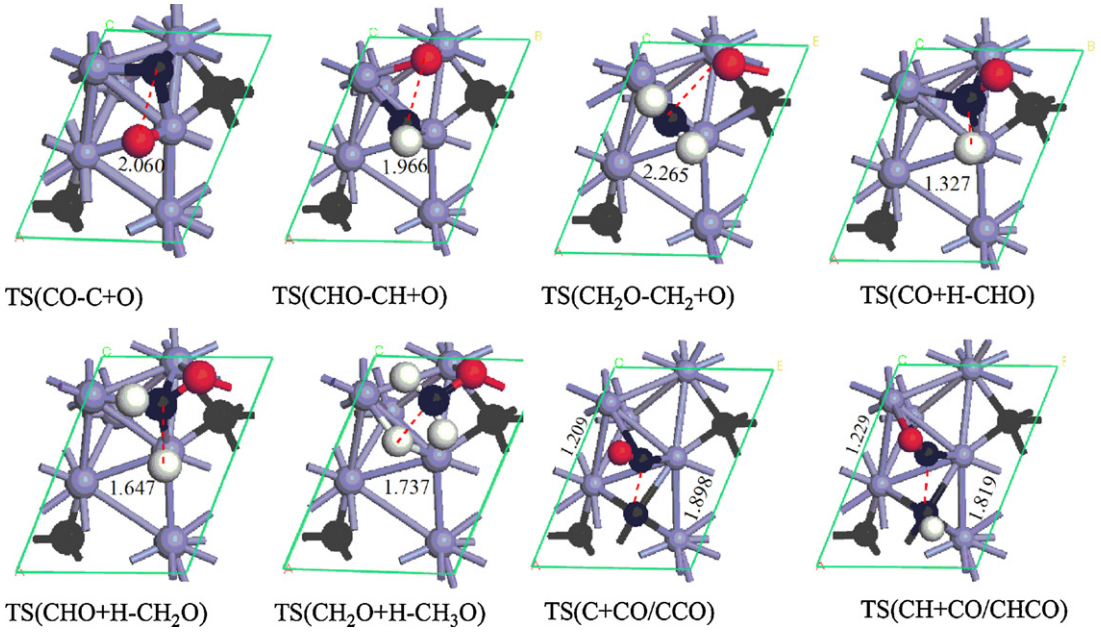

Fig. 3. Transition state structures of CO hydrogenation, dissociation and coupling on $Fe_5C_2(0\,0\,1)$.

Table 2
Computed activation energy and reaction energy (eV) of C_2–C_1 coupling on Fe_5C_2(0 0 1).

	ΔE[a]	$E_{a(f)}$[b]	$E_{a(r)}$[c]	$\Delta H_{(c)}$[d]
CO + CCO → COCCO (**5a**)	0.11	1.43	0.94	0.49
CH + CCO → CHCCO (**5b**)	0.13	1.71	1.66	0.05
C(a) → C(b) (**6a**)	0.00	0.62	0.61	0.01
C(b) → C(c) (**6b**)	0.00	0.97	0.24	0.73
$C_{(c)}$CCO → $C_{(a)}$CCO (**6c**)	0.00	0.32	1.30	−0.98
$C_{(a)}$ + CCO → $C_{(a)}$CCO (**7a**)	0.18	1.99	2.18	−0.19
$C_{(c)}$ + CCO → $C_{(c)}$CCO (**7b**)	0.19	0.53	0.60	−0.07
CCO + H → CHCO (**8a**)	0.19	0.75	0.39	0.36
CCO + H → CCHO (**8b**)	0.47	0.61	1.06	−0.45
CCO → CC + O (**9**)	0.37	1.93	2.04	−0.11
CHCO + H → CH_2CO (**10a**)	0.30	0.49	0.28	0.21
CHCO + H → $CHCHO_{(a)}$ (**10b**)	0.00	0.86	0.42	0.44
CCHO + H → CCH_2O (**10c**)	0.31	0.80	0.52	0.28
CCHO + H → $CHCHO_{(b)}$ (**10d**)	0.26	1.31	0.0	1.31
CHCO → $CCH_{(a)}$ + O (**11a**)	0.51	1.65	1.87	−0.22
CCHO → $CCH_{(b)}$ + O (**11b**)	0.34	1.22	1.54	−0.32
CHCHO + H → CH_2CHO (**12a**)	0.0	0.81	0.32	0.49
CCH_2O + H → $CHCH_2O$ (**12b**)	0.0	1.09	0.23	0.86
CH_2CO → $CCH_{2(a)}$ + O (**13a**)	0.05	0.43	1.64	−1.21
CHCHO → CHCH + O (**13b**)	0.43	0.39	1.09	−0.70
CCH_2O → $CCH_{2(b)}$ + O (**13c**)	0.03	0.82	1.55	−0.73

[a] For a reaction (A + B → AB), $\Delta E = [E(A + B/slab) + E(slab)] - (E(A/slab) + E(B/slab))$ for co-adsorbed A and B.
[b] $E_{a(f)} = [E(TS) + E(slab)] - (E((A + B)/slab)$ for the forward energy barrier.
[c] $E_{a(r)} = [E(TS) + E(slab)] - (E(AB/slab)$ for the reversed energy barrier.
[d] $\Delta H(c) = E(AB/slab) - E((A + B)/slab)$ for reaction energy.

(**5b**), CH and CO are adsorbed at 2-fold sites, respectively. The C–C distances are 2.239 and 2.029 Å, respectively.

For CCO + C reactions, there are two adsorption modes of CCCO, and also two co-adsorption modes of CCO vs. $C_{(a)}$ and CCO vs. $C_{(c)}$. The migration of $C_{(a)}$ and $C_{(c)}$ is a two-step process from $C_{(a)} \rightarrow C_{(b)} \rightarrow C_{(c)}$, and the barriers of the two steps are 0.62 and 0.97 eV, respectively. Since the reaction energy of $C_{(a)}$ migration (**6a** and **6b**) to $C_{(c)}$ is endothermic by 0.74 eV (equal to $E_{r(C_{(a)} \rightarrow C_{(b)})} + E_{r(C_{(b)} \rightarrow C_{(c)})}$), $C_{(a)}$ is more stable than $C_{(c)}$.

For the two sites of C(a and c) coupling with CCO (**7a** and **7b**), the lateral interaction of CCO and C(a and c) is 0.18 and 0.19 eV, and the barriers are 1.99 and 0.53 eV, respectively. In the transition state structures of CCO + C(a and c), C atoms are adsorbed at 2-fold and 3-fold sites, respectively; and the C–C distances are 2.148 and 1.858 Å, respectively. The migration $C_{(c)}$CCO to $C_{(a)}$CCO (**6c**) has low barrier (0.32 eV) and is exothermic (−0.98 eV). Thus, C atom migration is the first step, followed by the coupling with CCO atom and migration into another more stable mode; $CCO + C_{(a)} \rightarrow CCO + C_{(b)} \rightarrow CCO + C_{(c)} \rightarrow C_{(c)}CCO \rightarrow C_{(a)}CCO$. The effective barrier of this stepwise process is 1.61 eV, lower than the barrier of the one step reaction (2.17 eV).

For CCO hydrogenation and dissociation, the PES is shown in Fig. 6. Firstly, CCO + H → CHCO (**8a**)/CCHO (**8b**) are competitive, the lateral interaction of CCO and two-site H atom is 0.19 and 0.47 eV, and the barriers are 0.75 and 0.61 eV, respectively, and they are endothermic with 0.36 eV and exothermic with 0.45 eV, respectively). In the transition state structures of CCO + H → CHCO (**8a**)/CCHO (**8b**), H atom is adsorbed at top site in each case, and the C–H distance is 1.564 and 1.450 Å, respectively.

CCO dissociation into C_2 + O (9) has barrier of 1.93 eV and is exothermic (0.11 eV). The lateral interaction of co-adsorbed C_2 and O is 0.37 eV. Therefore, CCO hydrogenation is more favored. Secondly, the lateral interaction of CHCO and two-site H atoms is 0.30 and 0.0 eV, respectively. The barriers of CHCO hydrogenation into CH_2CO (**10a**) and $CHCHO_{(a)}$ (**10b**) are 0.49 and 0.86 eV, respectively, while that of CHCO dissociation into $CCH_{(a)}$ + O (**11a**) is higher (1.65 eV), and the lateral interaction of $CCH_{(a)}$ and O atom is 0.51 eV. CHCO hydrogenation is more preferable than dissociation.

The lateral interaction of co-adsorbed CCHO and two-site H atoms is 0.31 and 0.26 eV, respectively. The barrier of CCHO hydrogenation into CCH_2O (**10c**) is 0.80 eV, while CCHO hydrogenation into $CHCHO_{(b)}$ (**10d**) raises the energy with 1.31 eV, while the bar-

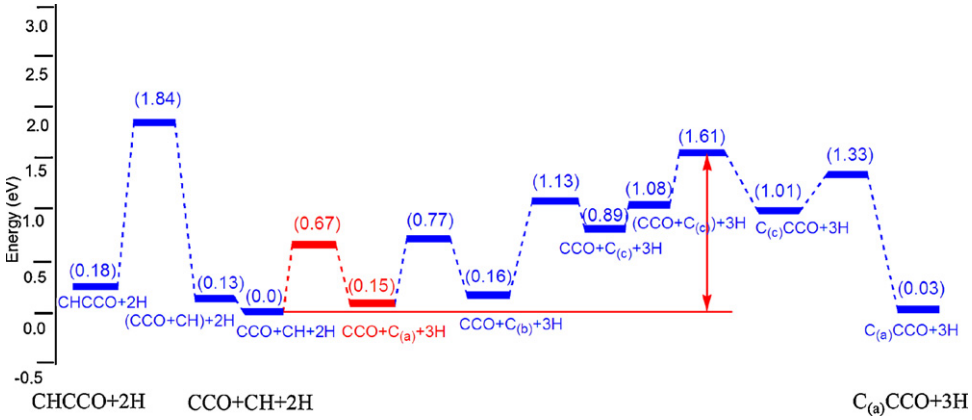

Fig. 4. Potential energy surface of CCO coupling (blue line) and CH dehydrogenation (red line) on Fe_5C_2(0 0 1). (For interpretation of the references to colour in this figure legend, the reader is referred to the web version of this article.)

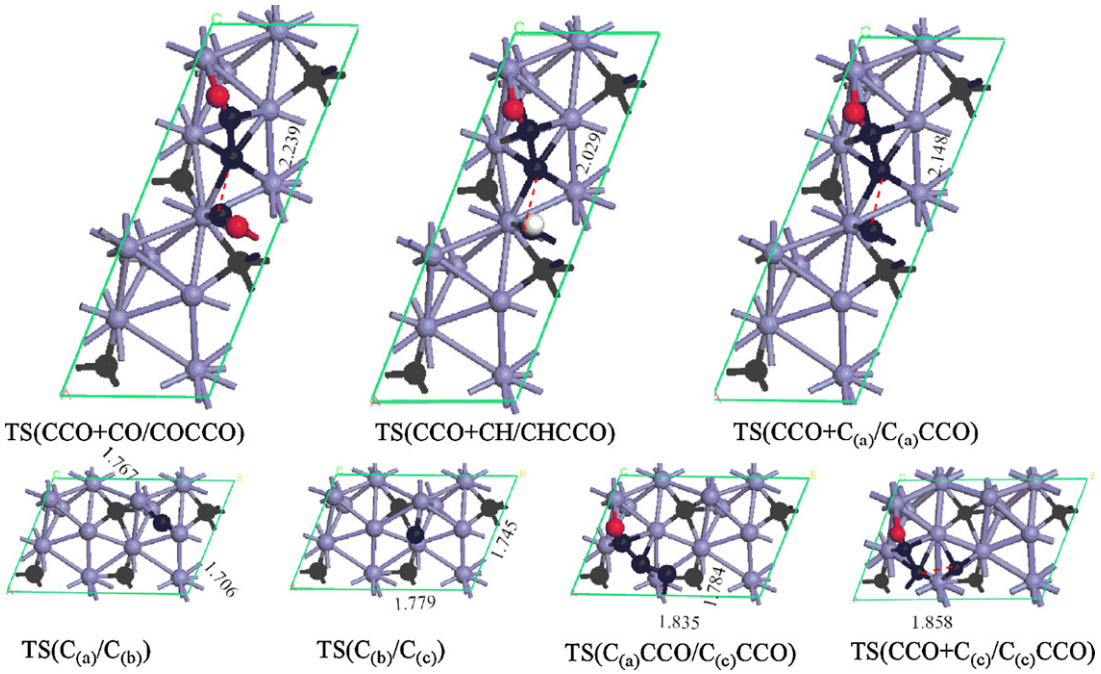

Fig. 5. Transition state structures of CCO coupling on $Fe_5C_2(0\,0\,1)$.

rier of CCHO dissociation into $CCH_{(b)}+O$ (**11b**) is 1.22 eV. Thus, CCHO hydrogenation into CCH_2O is favored.

For the third step, since CH_2CO dissociation into CH_2C+O (**13a**) is preferred over hydrogenation [47], $CCH_{2(a)}$ formation is favored. The lateral interaction between $CCH_{2(a)}$, CHCH, $CCH_{2(b)}$, and O atom is 0.05, 0.43, 0.03 eV, respectively. The barrier of CHCHO hydrogenation (**12a**) and dissociation (**13b**) is 0.81 and 0.39 eV, respectively; CHCHO dissociation into (CHCH + O) is preferred over hydrogenation. The barrier of CCH_2O hydrogenation (**12b**) and dissociation (**13c**) is 1.09 and 0.82 eV, respectively, $CCH_{2(b)}$ formation is also favored.

In the transition state structures of CCO, CHCO and CCHO dissociation, O atom is adsorbed at 2-fold in each case, and the C–O distance is 1.867, 2.239, and 2.000 Å, respectively. In the transition state structures of $CHCO+H\rightarrow CHCHO/CH_2CO$ and $CCHO+H\rightarrow CCH_2O$, H atom is adsorbed at top sites in each case, and the C–H distance is 1.324, 1.482 and 1.311 Å, respectively. Similarly, in the transition state structures of CHCHO and CCH_2O hydrogenation, H atom also is absorbed at top sites in each case, and the C–H distance is 1.498 and 1.431 Å, respectively. In the transition state structures of CHCHO, CH_2CO and CCH_2O dissociation, O atom is absorbed at 2-fold site in each case, and the C–O distance is 1.889, 1.811 and 1.981 Å, respectively.

For the initiation step, C + CO and C + H have low forward and reversed barrier (0.66 vs. 0.65, 0.52 eV vs. 0.67 eV). The forward and reversed rate constants of C + CO are 1.30×10^5 and $1.65\times10^5\ s^{-1}$ at 483 K, respectively, and the forward and reversed rate constants of C + H are 2.31×10^6 and $1.02\times10^5\ s^{-1}$ at 483 K, respectively. Furthermore, among all CH reaction pathways, CH + CO, CH + H, CH + CCO and C + CCO, the rate constant of $C_{(c)}$ + CCO is the largest with $2.95\times10^6\ s^{-1}$. Therefore, the most favored pathway is CH → C + H and C + CCO. On the other hand, among all CCO reaction

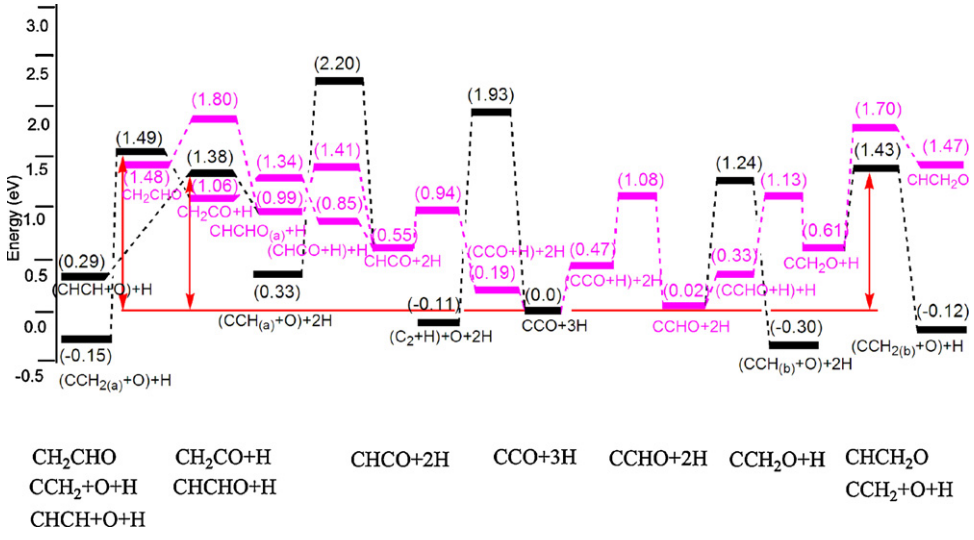

Fig. 6. Potential energy surface of CCO hydrogenation (pink line) and CCH_xO dissociation (black line) on $Fe_5C_2(0\,0\,1)$. (For interpretation of the references to colour in this figure legend, the reader is referred to the web version of this article.)

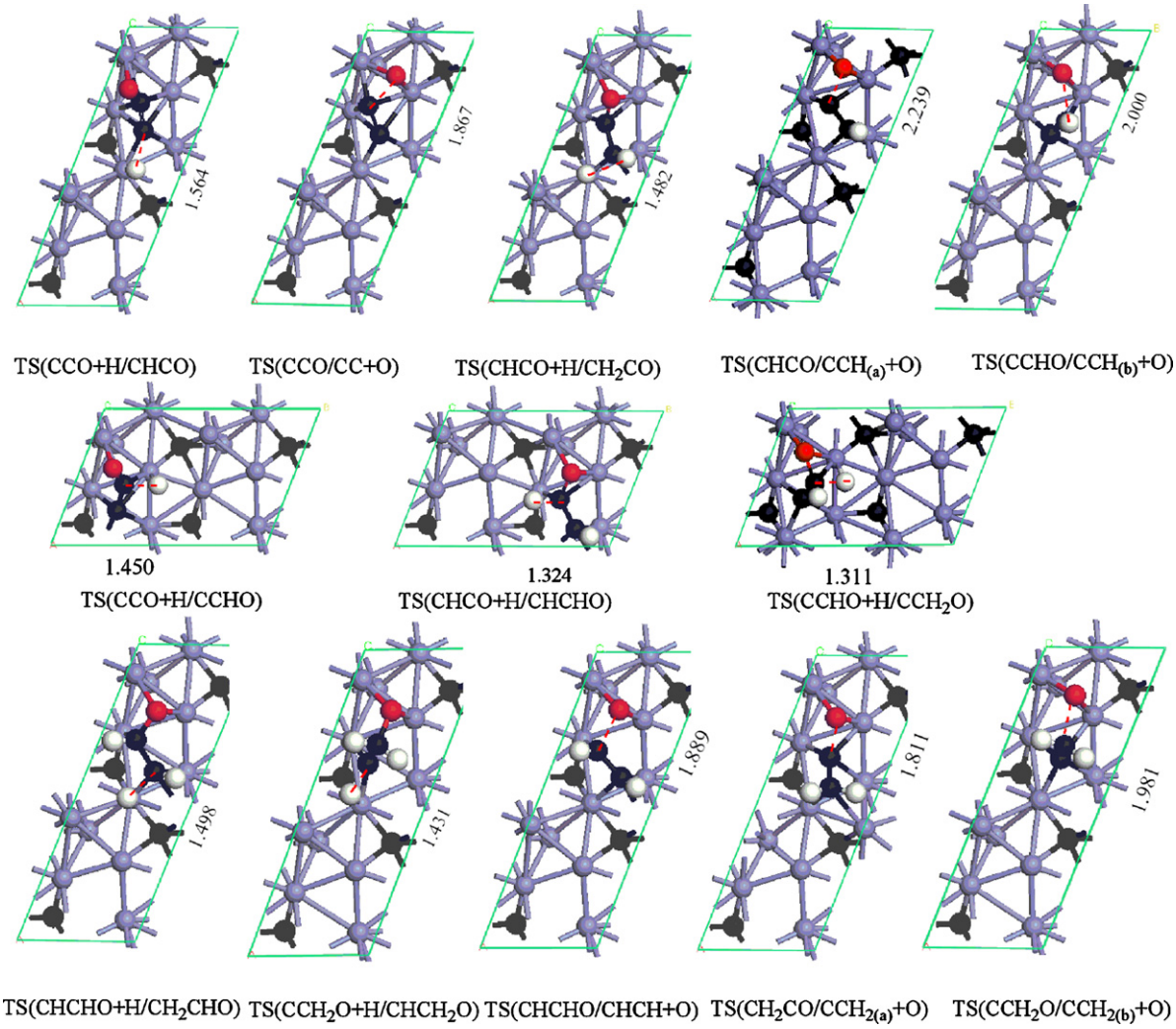

Fig. 7. Transition state structures of CCO hydrogenation and dissociation on $Fe_5C_2(0\,0\,1)$.

pathways, CCO + H, CCO + CO, CCO + CH and CCO + C, the rate constants of CCO + H → CHCO/CCHO and CCO + $C_{(c)}$ → $CCCO_{(b)}$ are high with 1.49×10^4, 4.31×10^5, and 2.95×10^6 s^{-1} (Table 3). Therefore, C + CO/CCO will not shift back to the left, while C + H/CH will shift back to the left to couple with CCO.

Consequently, the pathways of CCO hydrogenation and dissociation is CCO + 2H → CHCO + H → CH_2CO/CHCHO → $CCH_{2(a)}$/CHCH + O and CCO + 2H → CCHO + H → CCH_2O → $CCH_{2(b)}$ + O. The effective barrier of $CCH_{2(a)}$, $CCH_{2(b)}$, and CHCH formation is similar with 1.49, 1.38 and 1.43 eV, respectively, and the formation of $CCH_{2(a)}$, $CCH_{2(b)}$ and CHCH is preferable. Since the effective barrier of CCO coupling reactions of 1.61 eV is close to those of hydrogenation reactions, both CCO coupling and hydrogenation are possible along with CCCO, CCH_2 and CHCH as intermediates.

3.3. CCH_2 reaction pathway

For $CCH_{2(a)}$ coupling, hydrogenation and dehydrogenation, and CCH coupling and dehydrogenation, the barriers and reaction energies are shown in Table 4. The PES of CCH_2 reaction is shown in Fig. 8. The transition state structures are shown in Fig. 9. The coupling reactions of $CCH_{2(a)}$ + CH (**14a**) and $CCH_{2(a)}$ + (CO) (**14b**) are computed at first, and this is because that $CCH_{2(a)}$, CH and CO are the main species. The lateral interaction of co-adsorbed $CCH_{2(a)}$ and CH vs. CO is 0.14 and 0.10 eV, respectively. $CCH_{2(a)}$ + CH (**14a**) and $CCH_{2(a)}$ + CO (**14b**) have barriers of 1.10 and 0.86 eV, respectively, and are exothermic with 0.05 and endothermic with 0.54 eV, respectively, and the back reaction of $CCH_{2(a)}$ + CO is much easier. In addition, we investigated the $CCH_{2(a)}$ coupling with C atoms. Since

Table 3
The rate constants of hydrogenation and coupling reactions of CO species on $Fe_5C_2(0\,0\,1)$ at 483 and 543 K.

	k_f (s^{-1}), T = 483 K	k_r (s^{-1}), T = 483 K	k_f (s^{-1}), T = 543 K	k_r (s^{-1}), T = 543 K
C + H → CH	2.31×10^6	1.02×10^5	9.73×10^6	6.04×10^5
C + CO → CCO	1.30×10^5	1.65×10^5	7.48×10^6	9.27×10^5
CH + H → CH_2	5.7×10^3	6.18×10^{11}	4.65×10^4	6.52×10^{11}
CH + CO → CHCO	1.41×10^1	4.58×10^8	2.22×10^2	1.07×10^9
CH + CCO → CHCCO	1.43×10^{-6}	1.13×10^{-6}	1.34×10^{-4}	3.91×10^{-4}
CO + CCO → COCCO	1.19×10^{-3}	1.55×10^2	5.34×10^{-2}	1.88×10^3
$C_{(a)}$ + CCO → $CCCO_{(a)}$	1.72×10^{-9}	1.79×10^{-11}	3.38×10^{-7}	5.93×10^{-9}
$C_{(c)}$ + CCO → $CCCO_{(b)}$	2.95×10^6	5.49×10^5	1.20×10^7	2.69×10^6
CCO + H → CHCO	1.49×10^4	8.52×10^7	1.09×10^5	2.39×10^8
CCO + H → CCHO	4.31×10^5	3.32	2.01×10^6	6.17×10^1

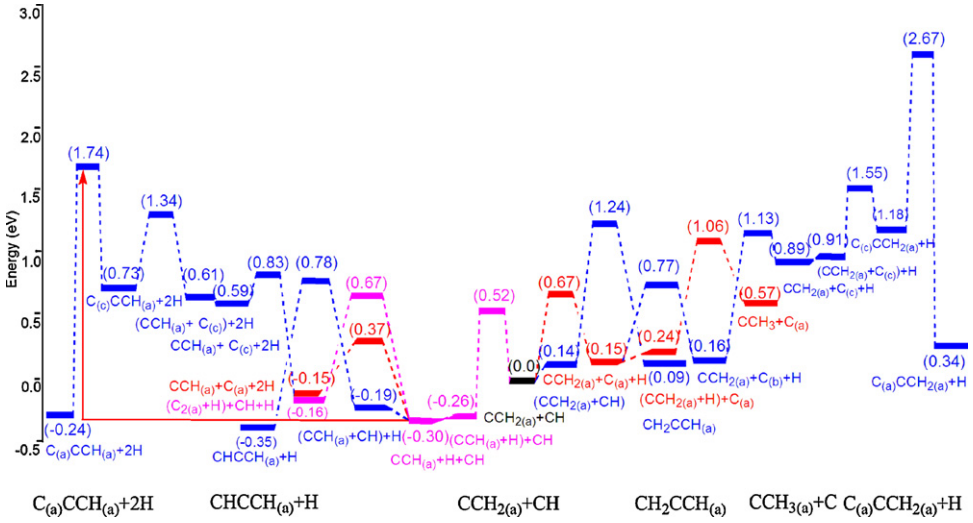

Fig. 8. Potential energy surface of $CCH_{2(a)}$ hydrogenation (red line, also CH dehydrogenation), dehydrogenation (pink line), and coupling (blue line). (For interpretation of the references to colour in this figure legend, the reader is referred to the web version of this article.)

there are two adsorbed modes of $CCCH_{2(a)}$, there are also two co-adsorption configurations of CCH_2 and C with the lateral interaction by 0.08 and 0.02 eV, respectively. For C_a (**15a**) and C_c (**15b**) coupling with $CCH_{2(a)}$, the barrier is 1.31 and 0.64 eV, respectively. The migration of $C_{(c)}CCH_{2(a)}$ to $C_{(a)}CCH_{2(a)}$ (**15c**) has barrier of 1.49 eV, and is exothermic (0.84 eV).

Compared with CCH_2 chain propagation, CCH_2 can also first dissociate into CCH, which can couple with CH, C or CO. The reaction pathway of CCH_2 hydrogenation, dehydrogenation and CCH coupling reactions are shown in Fig. 8; and the transition state structures are shown in Fig. 9. For the co-adsorbed CCH_2, H, and C species, there are two possible reaction pathways, one is CCH_2 hydrogenation, and the other is C migration ($C_{(a)} \rightarrow C_{(b)}$) followed by CCH_2 coupling. The lateral interaction of $CCH_{2(a)}$ and two-site H is 0.0 and 0.09 eV, respectively. $CCH_{2(a)} + H \rightarrow CHCH_2$ (**16a**) has no barrier, and $CCH_{2(a)} + H \rightarrow CCH_3$ (**16b**) has barrier of 0.82 eV, and they are endothermic (0.74 and 0.33 eV, respectively); therefore their back reactions are much easier. Compared with the barrier and reaction energy of $C_{(a)}$ migration (0.62/0.01 eV, Table 2), $C_{(a)}$ migration, instead of $CCH_{2(a)}$ hydrogenation, is favored. $CCH_{2(a)}$ dehydrogenation into $CCH_{(a)} + H$ (**16c**) has barrier of 0.52 eV, and is exothermic by 0.26 eV. The lateral interaction of $CCH_{(a)}$ and H is 0.04 eV. Compared with $CCH_{2(a)}$ coupling with CH/CO, $CCH_{2(a)}$ dehydrogenation into $CCH_{(a)}$ is more favored.

For CCH coupling with CH (**17a**), CO (**17b**) and $C_{(a,c)}$ (**18a**, **18b**), the lateral interaction of CCH with CH, CO, and $C_{(a,c)}$ is 0.11, 0.10, 0.07, 0.02 eV, respectively. $CCH + C_{(c)}$ has the lowest barrier (0.73 eV), compared to those of $CCH + CH/CO/C_{(a)}$ (0.97, 0.89 and 1.27 eV, respectively). The migration of $C_{(c)}CCH_{(a)}$ to $C_{(a)}CCH_{(a)}$ (**18e**) has barrier of 1.01 eV, and is exothermic by 0.97 eV. In addition, the barrier of CCH dehydrogenation into $C_{2(a)} + H$ (19) is 0.97 eV, higher than that of CCH coupling and hydrogenation (0.73 and 0.78 eV). The lateral interaction of $C_{2(a)}$ and H is 0.12 eV. Thus, CCH is preferred to couple with C atom. For the process of $CCH_{2(a)}$ dehydrogenation followed by coupling with C atom, the effective barrier of $C_{(a)}CCH_{(a)}$ is 2.04 eV. For co-adsorbed $CCH_{2(a)}$ and CH, the favored pathway is $CCH_2 + CH \rightarrow CCH + CH + H \rightarrow CCH + C + 2H \rightarrow CCCH + 2H$.

In the transition state structures of $CCH_{2(a)} + CH/CO/C(a, c)$, CH, CO, and C atoms are adsorbed at 2-fold sites, and the C-C distance is 2.169, 2.280, 2.036, and 1.862 Å, respectively. In the transition state structures of $CCH_{2(a)}$ hydrogenation and dehydrogenation reactions, the C–H distance is 1.439 and 1.467 Å, respectively. In the transition state structures of $CCH_{(a)} + CH/CO/C(a, c)$, CH and CO are adsorbed at 2-fold sites, while C atoms are adsorbed at 2-fold, and 3-fold sites, respectively; and the C–C distance is 2.287, 1.859, 2.036 and 1.805 Å, respectively. In the transition state structure of $CCH_{(a)}$ dehydrogenation, the C–H distance is 1.518 Å.

Table 4
Computed activation energy and reaction energy (eV) of $CCH_{2(a)}$ hydrogenation and C–C coupling of $CCH_{2(a)}$ on $Fe_5C_2(0\,0\,1)$.

	ΔE[a]	$E_{a(f)}$[b]	$E_{a(r)}$[c]	$\Delta H(c)$[d]
$CCH_{2(a)} + CH \rightarrow CHCCH_{2(a)}$ (**14a**)	0.14	1.10	1.15	−0.05
$CCH_{2(a)} + CO \rightarrow COCCH_{2(a)}$ (**14b**)	0.10	0.86	0.32	0.54
$CCH_{2(a)} + C_{(a)} \rightarrow C_{(a)}CCH_{2(a)}$ (**15a**)	0.08	1.31	1.45	−0.14
$CCH_{2(a)} + C_{(c)} \rightarrow C_{(c)}CCH_{2(a)}$ (**15b**)	0.02	0.64	0.37	0.27
$C_{(c)}CCH_{2(a)} \rightarrow C_{(a)}CCH_{2(a)}$ (**15c**)	0.00	1.49	2.33	−0.84
$CCH_{2(a)} + H \rightarrow CHCH_{2(a)}$ (**16a**)	0.00	0.74	0.0	0.74
$CCH_{2(a)} + H \rightarrow CCH_{3(a)}$ (**16b**)	0.09	0.82	0.49	0.33
$CCH_{2(a)} \rightarrow CCH_{(a)} + H$ (**16c**)	0.04	0.52	0.78	−0.26
$CCH_{(a)} + CH \rightarrow CHCCH_{(a)}$ (**17a**)	0.11	0.97	1.13	−0.16
$CCH_{(a)} + CO \rightarrow COCCH_{(a)}$ (**17b**)	0.10	0.89	0.29	0.60
$CCH_{(a)} + C(a) \rightarrow C_{(a)}CCH_{(a)}$ (**18a**)	0.07	1.27	1.51	−0.24
$CCH_{(a)} + C(c) \rightarrow C_{(c)}CCH_{(a)}$ (**18b**)	0.02	0.73	0.61	0.12
$C_{(c)}CCH_{(a)} \rightarrow C_{(a)}CCH_{(a)}$ (**18c**)	0.00	1.01	1.98	−0.97
$CCH_{(a)} \rightarrow C_{2(a)} + H$ (**19**)	0.12	0.97	0.83	0.14

[a] For a reaction ($A + B \rightarrow AB$), $\Delta E = [E(A + B/slab) + E(slab)] - (E(A/slab) + E(B/slab))$ for co-adsorbed A and B.
[b] $E_{a(f)} = [E(TS) + E(slab)] - (E((A + B)/slab)$ for the forward energy barrier.
[c] $E_{a(r)} = [E(TS) + E(slab)] - (E(AB/slab)$ for the reversed energy barrier.
[d] $\Delta H_{(c)} = E(AB/slab) - E((A + B)/slab)$ for reaction energy.

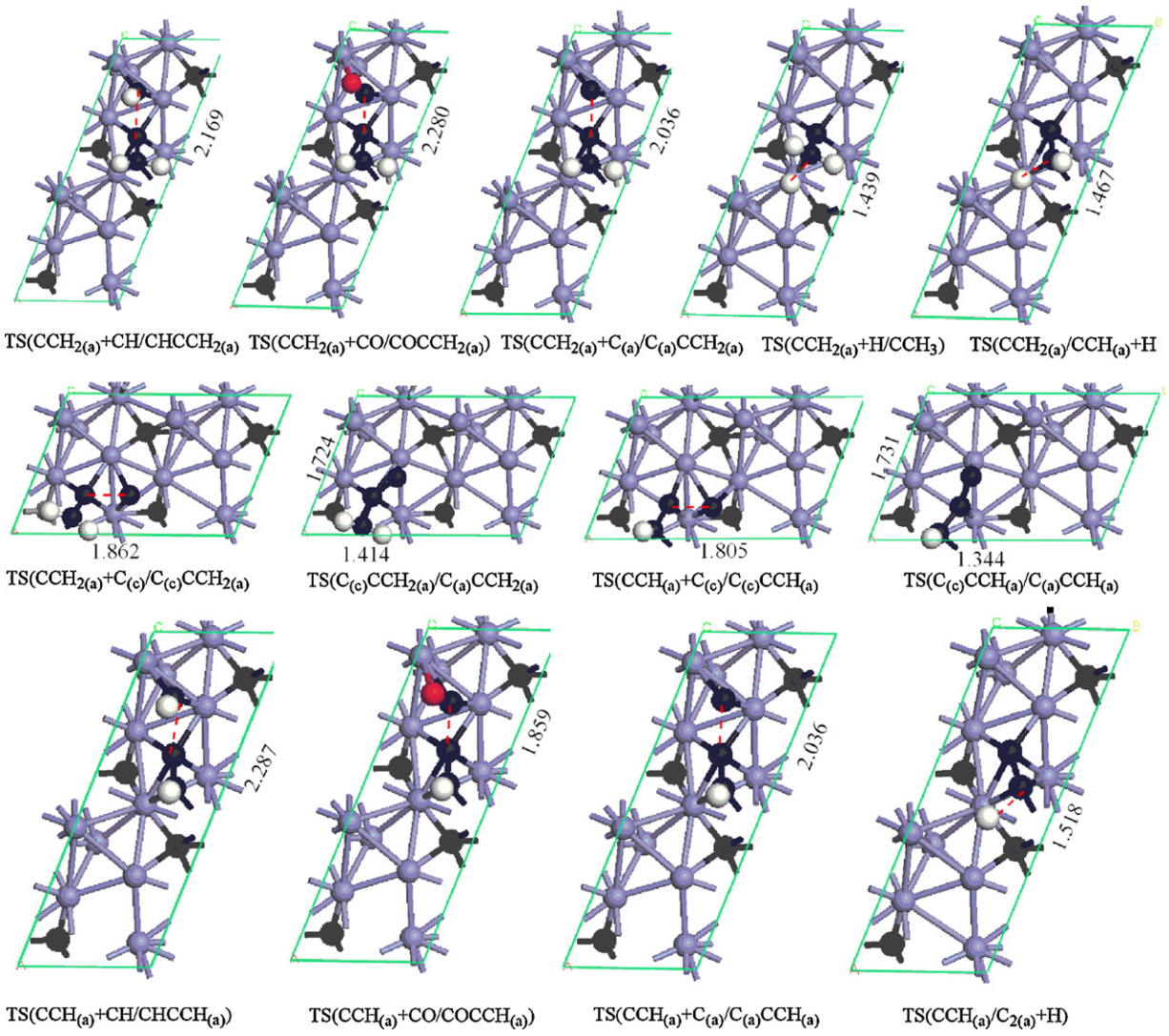

Fig. 9. Transition state structures of $CCH_{2(a)}$ hydrogenation, dehydrogenation and coupling on $Fe_5C_2(0\,0\,1)$.

For $CCH_{2(b)}$ coupling, hydrogenation and dehydrogenation, and CCH coupling and dehydrogenation, the barriers, reaction energies are given in Table 5. The potential energy surface of CCH_2 reaction is shown in Fig. 10, and the transition state structures are shown in Fig. 11. For the co-adsorbed $CCH_{2(b)}$, CH, and CO, the lateral interaction of $CCH_{2(b)}$ with CH and CO is 0.10 and 0.05 eV, respectively. $CCH_{2(b)} + CH$ (**20a**) and $CCH_{2(a)} + CO$ (**20b**) have barriers of 1.71 and 1.36 eV, respectively, and are endothermic (0.14 and 0.43 eV, respectively). In addition, we investigated $CCH_{2(a)}$ coupling with C atoms. Since there are two adsorbed modes of $CCCH_{2(b)}$, there are

Table 5
Computed activation energy and reaction energy (eV) of $CCH_{2(b)}$ hydrogenation and C–C coupling of $CCH_{2(b)}$ on $Fe_5C_2(0\,0\,1)$.

	ΔE[a]	$E_{a(f)}$[b]	$E_{a(r)}$[c]	$\Delta H_{(c)}$[d]
$CH + CCH_{2(b)} \rightarrow CHCCH_{2(b)}$ (**20a**)	0.10	1.71	1.57	0.14
$CO + CCH_{2(b)} \rightarrow COCCH_{2(b)}$ (**20b**)	0.05	1.36	0.93	0.43
$C_{(a)} + CCH_{2(b)} \rightarrow C_{(a)}CCH_{2(b)}$ (**21a**)	0.11	2.12	2.49	−0.37
$C_{(c)} + CCH_{2(b)} \rightarrow C_{(c)}CCH_{2(b)}$ (**21b**)	0.00	1.16	1.43	−0.27
$C_{(c)}CCH_{2(b)} \rightarrow C_{(a)}CCH_{2(b)}$ (**21c**)	0.00	0.37	1.08	−0.71
$CCH_{2(b)} + H \rightarrow CCH_{3(b)}$ (**22a**)	0.04	0.68	0.37	0.31
$CCH_{2(b)} \rightarrow CCH_{(b)} + H$ (**22b**)	0.08	1.00	1.23	−0.23
$CH + CCH_{(b)} \rightarrow CHCCH_{(b)}$ (**23a**)	0.11	1.72	1.70	0.02
$CO + CCH_{(b)} \rightarrow COCCH_{(b)}$ (**23b**)	0.06	1.42	0.94	0.48
$C_{(a)} + CCH_{(b)} \rightarrow C_{(a)}CCH_{(b)}$ (**23c**)	0.10	2.10	2.45	−0.35
$C_{(c)} + CCH_{(b)} \rightarrow C_{(c)}CCH_{(b)}$ (**23d**)	0.00	0.76	1.02	−0.26
$C_{(c)}CCH_{(b)} \rightarrow C_{(a)}CCH_{(b)}$ (**23e**)	0.00	0.67	1.52	−0.85
$CCH_{(b)} \rightarrow C_{2(b)} + H$ (**24**)	0.21	1.37	0.73	0.64

[a] For a reaction $(A + B \rightarrow AB)$, $\Delta E = [E(A + B/slab) + E(slab)] - (E(A/slab) + E(B/slab))$ for co-adsorbed A and B.
[b] $E_{a(f)} = [E(TS) + E(slab)] - (E((A + B)/slab)$ for the forward energy barrier.
[c] $E_{a(r)} = [E(TS) + E(slab)] - (E(AB/slab)$ for the reversed energy barrier.
[d] $\Delta H_{(c)} = E(AB/slab) - E((A + B)/slab)$ for reaction energy.

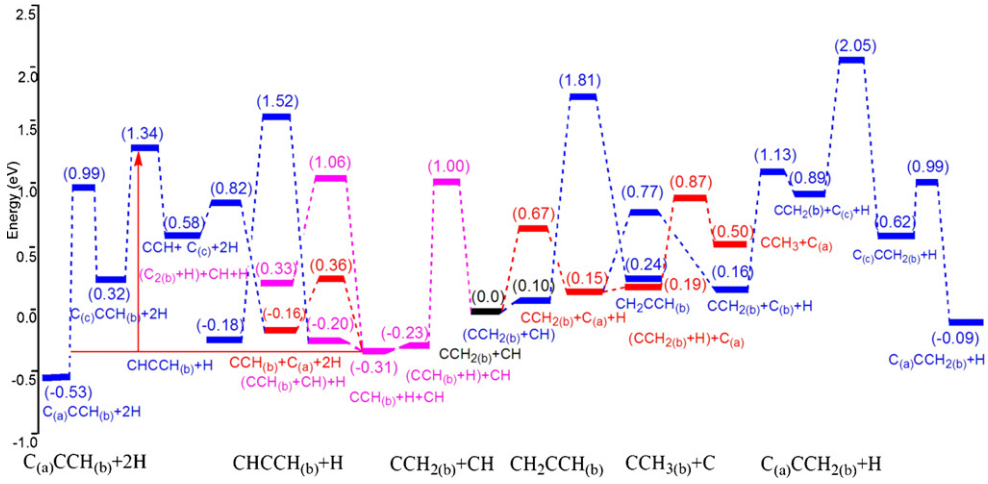

Fig. 10. Potential energy surface of $CCH_{2(b)}$ hydrogenation (red line, also CH dehydrogenation), dehydrogenation (pink line), and coupling (blue line) on $Fe_5C_2(0\,0\,1)$. (For interpretation of the references to colour in this figure legend, the reader is referred to the web version of this article.)

also two co-adsorption modes of CCH_2 and C(a,c) with the lateral interaction by 0.11 and 0.0 eV, respectively. For $CCH_{2(b)} + C_{(a)}$ (**21a**) and $CCH_{2(b)} + C_{(c)}$ (**21b**), the barrier is 2.12 and 1.16 eV, respectively; while $C_{(c)}CCH_{2(a)}$ to $C_{(a)}CCH_{2(a)}$ (**21c**) migration has low barrier of 0.37 eV, and is exothermic (0.71 eV).

For the co-adsorbed $CCH_{2(b)}$, H and $C_{(a)}$ species, there are also two possible reaction pathways, one is $CCH_{2(b)}$ hydrogenation and the other one is C migration ($C_{(a)} \rightarrow C_{(b)}$) followed by CCH_2 coupling. The lateral interaction of $CCH_{2(b)}$ and H is 0.04 eV. $CCH_{2(b)} + H \rightarrow CCH_3$ (**22a**) has barrier of 0.68 eV, and is endothermic with 0.31 eV, and the back reaction is much easier. The energy barrier and reaction energy of $C_{(a)}$ to $C_{(b)}$ migration (**6a**) is 0.62 and 0.01 eV, respectively. This indicates $C_{(a)}$ migration is more favored than $CCH_{2(b)}$ hydrogenation.

For the co-adsorbed $CCH_{2(b)}$ and CH species, $CCH_{2(b)}$ coupling with CH and dehydrogenation have been calculated. The energy barrier of $CCH_{2(b)} \rightarrow CCH_{(b)} + H$ (**22b**) is 1.00 eV, lower than that of $CCH_{2(a)}$ coupling with CH (1.10 eV, **14a**) and higher than that of CH dehydrogenation (0.67 eV). The lateral interaction of $CCH_{(b)}$ and H is 0.08 eV. $CCH_{2(b)}$ dehydrogenation is exothermic with 0.23 eV, while $CCH_{2(b)}$ coupling with CH and CH dehydrogenation are endothermic with 0.14 and 0.15 eV, respectively.

The lateral interaction of $CCH_{(b)}$ with CH, CO, and $C_{(a)}$ atom is 0.11, 0.06, and 0.10 eV, respectively, while there is no lateral interaction of $CCH_{(b)}$ and $C_{(c)}$. $CCH_{(b)} + CH$ (**23a**) and $CCH_{(b)} + CO$ (**23b**) couplings have barriers of 1.72 and 1.42 eV, respectively, and are endothermic with 0.02 and 0.48 eV, respectively. $CCH_{(b)} + C_{(c)}$ (**23d**) coupling has much lower barrier than $CCH_{(b)} + C_{(a)}$ (**23c**) coupling (0.76 eV vs. 2.10 eV). The migration of $C_{(c)}CCH_{(a)}$ to $C_{(a)}CCH_{(a)}$ (**23e**) has barrier of 0.67 eV, and is exothermic (0.85 eV). Thus, the pathway of $CCH_{(b)}$ coupling is $C_{(a)} \rightarrow C_{(b)} \rightarrow C_{(c)}$, $CCH_{2(b)} + C_{(c)} \rightarrow C_{(c)}CCH_{(b)} \rightarrow C_{(a)}CCH_{(b)}$. In addition, CCH dehydrogenation (**24**) has barrier of 1.37 eV, higher than that of CCH coupling and hydrogenation (0.76 and 1.23 eV). The lateral interaction of $C_{2(b)}$ and H is 0.21 eV. Thus, CCH is preferred to coupling with C atom. For the reaction of $CCH_{2(b)}$, the effective barrier of $C_{(a)}CCH_{(b)}$ formation is 1.65 eV, lower than that of $C_{(a)}CCH_{2(b)}$ formation (2.04 eV). Thus, $C_{(a)}CCH_{(b)}$ formation is favored. Consequently, $CCH_{2(a)}$ and $CCH_{2(b)}$ are favored to couple with C.

In the transition state structures of $CCH_{2(b)} + CH/CO/C_{(a,c)}$, CH, CO and C atoms are adsorbed at 2-fold sites, and the C–C distance is 2.050, 1.829, 2.051 and 2.021 Å, respectively. In the transition state structures of $CCH_{2(b)}$ hydrogenation and dehydrogenation reactions, the C–H distance is 1.516 and 1.655 Å, respectively. In the transition state structures of $CCH_{(a)} + CH/CO/C(a,c)$, CH and CO are adsorbed at 2-fold sites, while C atoms are adsorbed at 2-fold, and 3-fold sites, respectively. The C–C distance is 2.077, 1.888, 2.130 and 1.830 Å, respectively. In the transition state structure of $CCH_{(b)}$ dehydrogenation, the C–H distance is 1.580 Å.

3.4. CHCH reaction pathway

For CHCH coupling, hydrogenation, and dehydrogenation reactions, the barriers, reaction energies are shown in Table 6, and the transition state structures are shown in Fig. 12. The lateral interaction of CHCH with CH and H are both 0.10 eV, while there is no lateral interaction of CHCH and CO. CHCH + CO/CH (**25a**, **25b**) have very high barrier of 1.99 and 2.11 eV, and CHCH + H (**25c**) has barrier of 0.72 eV, and both reactions are endothermic. In contrast, CHCH dehydrogenation into $CCH_{(b)}$ (**25d**) has lower barrier (0.52 eV) and is exothermic (−0.76 eV). The lateral interaction of $CCH_{(b)}$ and H is 0.04 eV. In addition, The adsorption energy of CHCH is −2.88 eV, similarly, the adsorption energies of CHCH on Pt(1 1 1) and (2 1 1) are −2.87 eV and −2.83 eV [72]. Therefore, the direction desorption of CHCH need 2.88 eV, and this is rather difficult. Compared with CHCH hydrogenation, dehydrogenation, desorption, and coupling with CH and CO, the CHCH dehydrogenation is the most favored.

In the transition state structure of CHCH + CO/CH, CO and CH are adsorbed at 2-fold sites, the C–C distance is 2.055 and 2.080 Å. In the transition state structures of CHCH hydrogenation and dehydrogenation reactions, the C–H distance is 1.490 and 1.581 Å, respectively.

3.5. CO adsorption and dissociation on the vacancy sites

During surface C hydrogenation and coupling, vacancy sites will emerge on $Fe_5C_2(0\,0\,1)$ surface, and filling the vacancy sites is the key step to regenerate the active sites and maintain the catalyst stability. Therefore CO adsorption and dissociation on the vacancy sites are investigated. The energy data on the vacancy $Fe_5C_2(0\,0\,1)$ are listed in Table 7, and the transition state structures of CO dissociation and hydrogenation are shown in Fig. 13. CO is adsorbed at 4-fold vacancy site ($CO_{(v)}$), and the adsorption energy is −2.29 eV. For comparison, the adsorption energy of CO on perfect $Fe_5C_2(0\,0\,1)$ is −2.10 eV [73]. The barrier of CO dissociation and hydrogenation at vacancy site (**1a•**, **1b•**) is 1.16 and 0.77 eV, respectively, much lower than those (2.98 and 1.39 eV) on the perfect surface (**1a**, **1b**). Under surface CCH_2 co-adsorption, CO dissociation at vacancy site has barrier of 1.21 eV, and is exothermic by 0.39 eV. For comparison, CO dissociation without co-adsorbed CCH_2 has barrier of

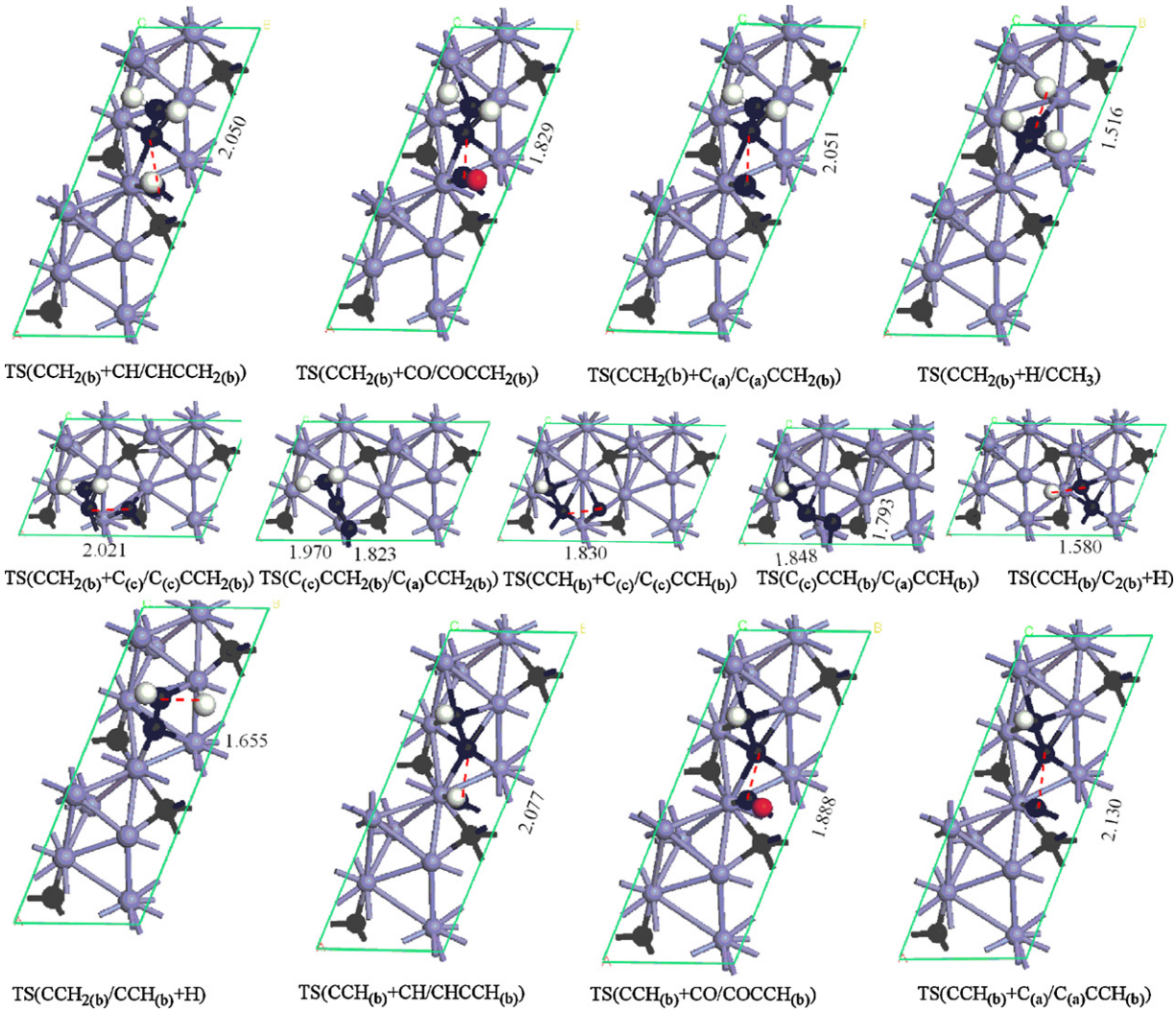

Fig. 11. Transition state structures of $CCH_{2(b)}$ hydrogenation, dehydrogenation and coupling on $Fe_5C_2(0\,0\,1)$.

Table 6
Computed activation energy and reaction energy (eV) of CHCH hydrogenation and C–C coupling of CHCH on $Fe_5C_2(0\,0\,1)$.

	ΔE[a]	$E_{a(f)}$[b]	$E_{a(r)}$[c]	$\Delta H_{(c)}$[d]
CHCH + CO → COCHCH (**25a**)	0.00	1.99	1.36	0.63
CHCH + CH → CHCHCH (**25b**)	0.10	2.11	1.90	0.21
CHCH + H → $CHCH_2$ (**25c**)	0.10	0.72	0.28	0.44
CHCH → $CCH_{(b)}$ + H (**25d**)	0.04	0.52	1.28	−0.76

[a] For a reaction (A + B → AB), $\Delta E = [E(A + B/slab) + E(slab)] - (E(A/slab) + E(B/slab))$ for co-adsorbed A and B.
[b] $E_{a(f)} = [E(TS) + E(slab)] - (E((A + B)/slab)$ for the forward energy barrier.
[c] $E_{a(r)} = [E(TS) + E(slab)] - (E(AB/slab)$ for the reversed energy barrier.
[d] $\Delta H_{(c)} = E(AB/slab) - E((A + B)/slab)$ for reaction energy.

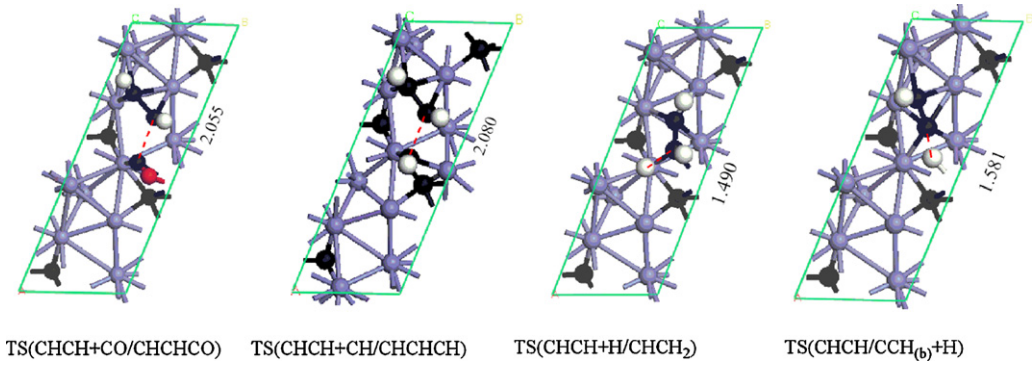

Fig. 12. Transition state structures of CHCH hydrogenation, dehydrogenation and coupling on $Fe_5C_2(0\,0\,1)$.

Table 7
Computed activation energy and reaction energy (eV) of $CH_xO_{(v)}$ hydrogenation and C–O cleavage of $CH_xO_{(v)}$ species on the vacancy $Fe_5C_2(0\,0\,1)$.

	ΔE[a]	$E_{a(f)}$[b]	$E_{a(r)}$[c]	$\Delta H_{(c)}$[d]
$CO_{(v)} \rightarrow C + O$ (**1a•**)	0.11	1.16	1.63	−0.47
$CO_{(v)} + H \rightarrow HCO_{(v)}$ (**1b•**)	0.0	0.77	0.03	0.74
$CHO_{(v)} \rightarrow CH + O$ (**2a•**)	0.13	0.74	2.11	−1.37
$CHO_{(v)} + H \rightarrow CH_2O_{(v)}$ (**2b•**)	0.0	1.30	0.44	0.86

[a] For a reaction (A + B → AB), $\Delta E = [E(A + B/slab) + E(slab)] - (E(A/slab) + E(B/slab))$ for co-adsorbed A and B.
[b] $E_{a(f)} = [E(TS) + E(slab)] - (E((A + B)/slab)$ for the forward energy barrier.
[c] $E_{a(r)} = [E(TS) + E(slab)] - (E(AB/slab)$ for the reversed energy barrier.
[d] $\Delta H_{(c)} = E(AB/slab) - E((A + B)/slab)$ for reaction energy.

1.16 eV, and is exothermic by 0.47 eV. Therefore, the co-adsorbed CCH_2 species has almost no influence on CO dissociation. The barrier of CHO dissociation at vacancy site (**2a•**) is 0.74 eV, lower than that (1.16 eV) on the perfect surface (**2a**). However, the barrier of CHO hydrogenation at vacancy site (**2b•**) is 1.30 eV, higher than that (0.91 eV) on the perfect surface (**2b**). The lateral interaction of C and CH with O is 0.11 and 0.13 eV, respectively, and there are no lateral interaction of $CO_{(v)}$ and $CHO_{(v)}$ with H atoms. Since CO dissociation barrier (1.16 eV) at vacancy site (**1a•**) is higher than that (0.77 eV) of CO hydrogenation (**1b•**), CO at vacancy site is preferred to be hydrogenated into CHO. Furthermore, the barrier (0.74 eV) of CHO dissociation (**2a•**) is lower than that that (1.30 eV) of CHO hydrogenation (**2b•**). As a result, CHO at vacancy site is favored to dissociate into CH and O. This indicates that CO at vacancy sites is favored to form CH by hydrogenation and dissociation. Compared with CO adsorbed on the perfect $Fe_5C_2(0\,0\,1)$, CO at vacancy site is more preferred to adsorption, activation, hydrogenation and dissociation. This suggests that CO filling at vacancy site promotes the regeneration of the active site and sustain the catalytic cycle.

3.6. Removal of surface O and H_2O formation

Apart from the formation of surface hydrocarbons, water is a major by-product in FTS. Therefore, not only surface hydrocarbons but also surface oxygen, surface hydroxyl and surface water are important species in FTS. H_2O formation and removal can also promote the regeneration of the active site. The energy data of H_2O formation are listed in Table 8, and the transition state structures of oxygen hydrogenation are shown in Fig. 14. From CCH_2O dissociation, there are 3-fold O atom and CCH_2 on $Fe_5C_2(0\,0\,1)$. For OH adsorption, three adsorption modes of OH_{2f}, OH_{3f}, and OH_{4f} at 2-fold, 3-fold, and 4-fold sites are found, and the adsorption energy is −3.85, −3.68 and −3.25 eV, respectively. The OH adsorption energy at hcp, edge-bridge and near-edge-hcp sites on flat and stepped Co(0 0 0 1) is −3.45, −3.98 and −3.67 eV, respectively [74]. For H_2O adsorption, one mode at top site is obtained, and the adsorption

Table 8
Computed activation energy and reaction energy (eV) of H_2O formation on $Fe_5C_2(0\,0\,1)$.

	ΔE[a]	$E_{a(f)}$[b]	$E_{a(r)}$[c]	$\Delta H_{(c)}$[d]
$O_{4f} + H \rightarrow OH_{2f}$	0.0	1.70	1.30	0.40
$O_{3f} + H \rightarrow OH_{3f}$	0.0	1.53	0.90	0.63
$O_{4f} + H \rightarrow OH_{4f}$	0.0	1.67	0.57	1.10
$O_{3f} + O_{4f} + H \rightarrow OH_{2f} + O_{3f}$	0.16	1.48	1.31	0.17
$O_{3f} + O_{4f} + H \rightarrow OH_{3f} + O_{4f}$	0.84	0.80	1.23	−0.43
$OH_{2f} + O_{4f} + H \rightarrow H_2O + O_{4f}$	0.48	1.03	0.99	0.04
$OH_{3f} + OH_{4f} \rightarrow H_2O + O_{4f}$	0.0	0.21	0.29	−0.08

[a] For a reaction (A + B → AB), $\Delta E = [E(A + B/slab) + E(slab)] - (E(A/slab) + E(B/slab))$ for co-adsorbed A and B.
[b] $E_{a(f)} = [E(TS) + E(slab)] - (E((A + B)/slab)$ for the forward energy barrier.
[c] $E_{a(r)} = [E(TS) + E(slab)] - (E(AB/slab)$ for the reversed energy barrier.
[d] $\Delta H_{(c)} = E(AB/slab) - E((A + B)/slab)$ for reaction energy.

energy is −0.87 eV. Therefore, H_2O desorption needs 0.87 eV. For the formation of OH_{2f}, OH_{3f}, and OH_{4f}, the energy barrier is 1.70, 1.53 and 1.67 eV, respectively, and the reaction is endothermic by 0.40, 0.63 and 1.10 eV, respectively. There are no lateral interactions between O and H atoms for OH_{2f}, OH_{3f}, and OH_{4f} formation. Without adsorbed CCH_2, OH_{3f} formation has barrier of 1.41 eV, and is endothermic by 0.67 eV. Thus, oxygen hydrogenation into OH at low coverage is difficult. With the increasing of the coverage, OH_{2f} formation has barrier of 1.48 eV and is endothermic by 0.17 eV. The lateral interaction between 2-fold H and 4-fold O is 0.16 eV. For OH_{3f} formation, the energy barrier is 0.80 eV, and the reaction is exothermic by 0.43 eV. The lateral interaction between 3-fold O and 2-fold H is 0.84 eV. Thus, OH_{3f} formation is favored at high coverage of O atoms. For H_2O formation, there are two pathways with OH hydrogenation ($OH + H \rightarrow H_2O$) and disproponation ($2OH \rightarrow H_2O + O$). There is strong lateral interaction between 2-fold OH and 2-fold H with 0.48 eV. OH hydrogenation has barrier of 1.03 eV, and is endothermic by 0.04 eV. In contrast, there is no lateral interaction between 2-fold OH_{2f} and 4-fold OH_{4f}; and the OH disproponation has low barrier of 0.21 eV, and is exothermic by 0.08. Similarly H_2O formation by OH + OH has low barrier with

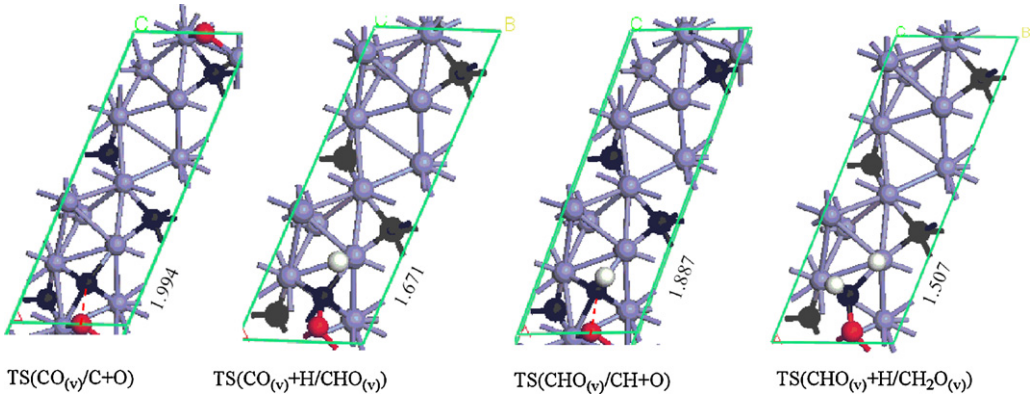

Fig. 13. Transition state structures of hydrogenation and dissociation of CO at vacancy site ($CO_{(v)}$) on $Fe_5C_2(0\,0\,1)$.

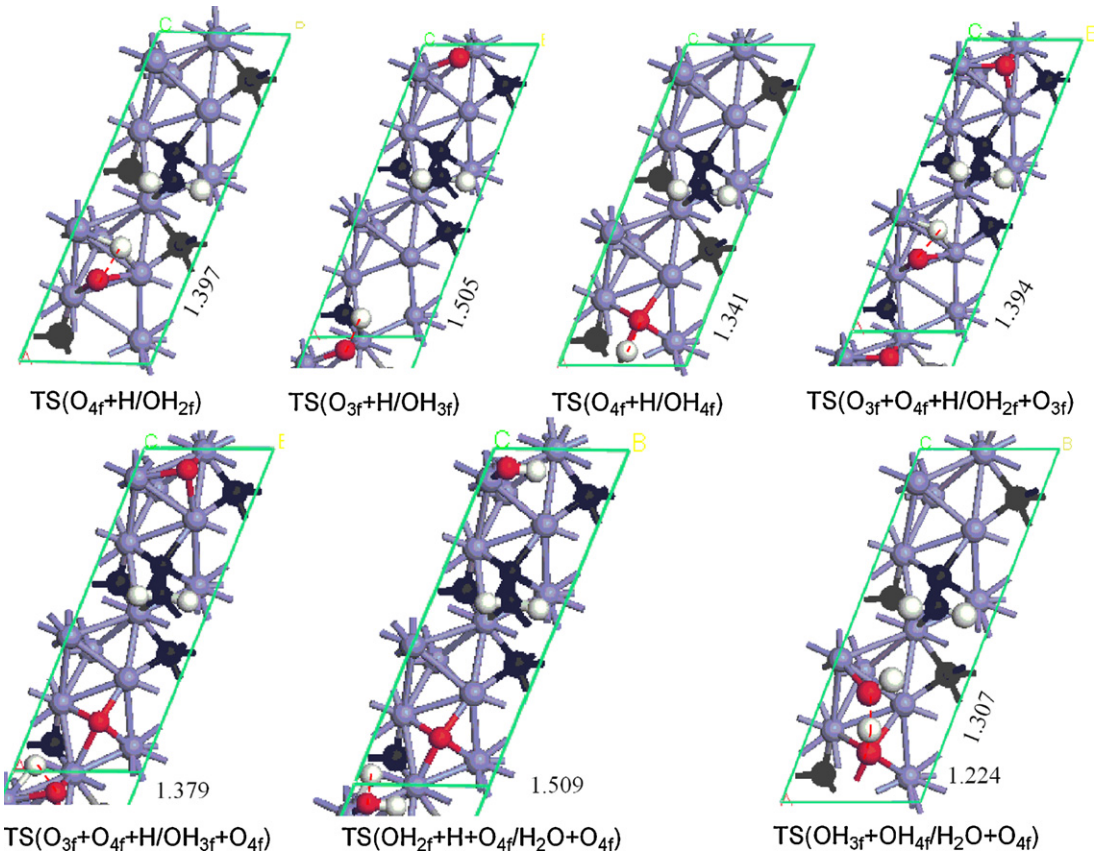

Fig. 14. The whole kinetic energy diagram connecting the reactants (CO, H, and surface C) and main C_3 intermediate (CCCO, CCCH).

0.64 eV on stepped Co(0 0 0 1) [59]. Therefore, OH disproponation to form H_2O is energetically more favored than OH hydrogenation.

3.7. Discussion

On the basis of our above calculations, the complete kinetic energy diagram is shown in Fig. 15. In order to simplify the elementary steps, the effective barriers are used in the steps of CCO hydrogenation and coupling, and CCH_2 and CHCH coupling. The first step of carbon chain formation on Fe_5C_2(0 0 1) is CO insertion into surface C to form CCO, which belongs to CO insertion mechanism. On the other hand, C hydrogenation into CH is also favored. Therefore, CCO and CH are the main species in the first FTS reaction step. Since CCO + CH has high barrier and one-step coupling is not favored, the stepwise pathway of CH dehydrogenation into C, following by CCO coupling form CCCO. On the other hand, CCO hydrogenation can also occur. CCO hydrogenation and C–O cleavage reactions are favored to form CCH_2 and CHCH.

For CCH_2, the favored pathway is CCH_2 dehydrogenates into CCH, followed by coupling with C to form CCCH. CHCH also is preferred to dehydrogenate into CCH. Along with CCO and CCH coupling with C/CH/CO, surface C atom is the most preferred C_1 species. This is similar with the favored chain propagation reaction with C + CCH_2 on Fe(1 0 0) [39]. For CCH_2 dehydrogenation and coupling, this step belongs to carbide mechanism. This suggests CO insertion mechanism and carbide mechanism indeed co-exist.

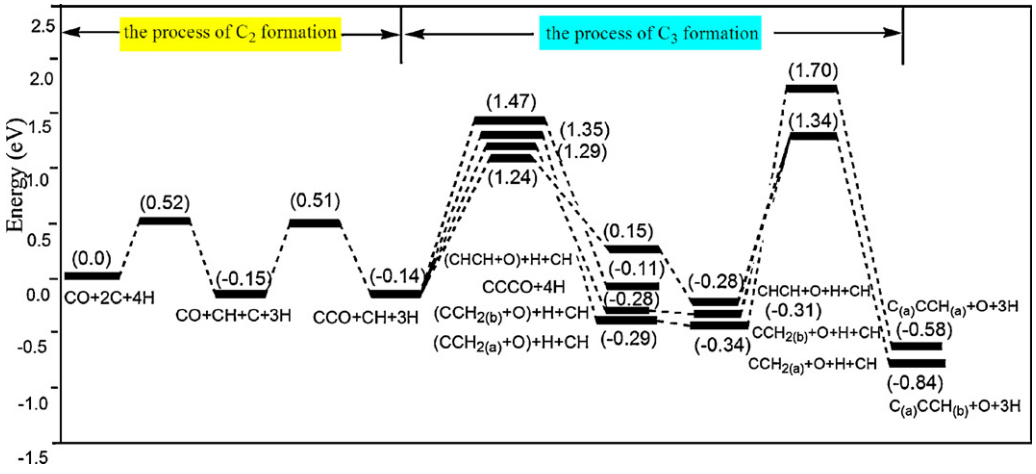

Fig. 15. The whole kinetic energy diagram connecting the reactants (CO, H, and surface C) and main C3 intermediate (CCCO, CCCH).

Table 9
The comparison of reaction energy and energy barriers of C + CO → CCO coupling on iron carbide surfaces.

FeC_x	Surface	E_a (eV)	ΔH (eV)	Ref.
Fe_2C	(0 1 1)	0.93	0.87	[77]
Fe_3C	(0 0 1)	1.89	1.05	[77]
Fe_4C	(1 0 0)	0.64	0.62	[77]
Fe_5C_2	(0 1 0) (0.25)[a]	2.04	0.84	[77]
Fe_5C_2	(0 1 0) (0.25)[a]	–	0.81	[78]
Fe_5C_2	(1 $\bar{1}$ $\bar{1}$)(0.0)[b]	–	0.45	[78]
Fe_5C_2	(1 1 0) (0.0)[b]	–	0.38	[78]
Fe_5C_2	(1 1 1) (0.0)[b]	–	0.62	[78]
Fe_5C_2	(1 $\bar{1}$ $\bar{1}$)(0.50)[c]	–	0.99	[78]
Fe_5C_2	(1 1 0) (0.50)[c]	–	0.50	[78]
Fe_5C_2	(0 0 1)	0.66	0.01	This paper
Fe_3C	(1 0 0)	–	−0.02	[80]

[a] 0.25 means a 0.25 fractional distance along with the normal axis.
[b] 0.0 means a 0.0 factional distance along the normal axis.
[c] 0.50 means a 0.50 fractional distance along with the normal axis.

For oxygenated and hydrocarbon intermediates of C_2 species, CCO, CCH_2 and CHCH are preferred to chain propagation into CCCO and CCCH. Thus, CCO is preferred to hydrogenation and coupling with C into CCCH when H_2/CO ratio is up to 1, while CCO is favored to occur chain propagation reaction to form CCCO when H_2/CO ratio is lower than 1. CCCO and CCCH are main C_3 intermediates. However, the H_2/CO ratio likely increases if CCCO transfers into hydrocarbon intermediate due to the increasing number of carbon. For the hydrogenation and coupling reactions of CCCO and CCCH will be paid attention in our future studies.

It is now interesting to compare CCO formation on Fe_5C_2(0 0 1) with other Fe_5C_2 surfaces and iron carbide surfaces (Table 9). For Fe_5C_2, the surface energies of (0 1 0)(0.25), (1 $\bar{1}$ $\bar{1}$)(0.0), (1 1 0)(0.0), (1 1 1)(0.0), (1 $\bar{1}$ $\bar{1}$)(0.50), (1 1 0)(0.50) are all lower than that of (0 0 1)(0.0) [75]. This indicates that the former six surfaces are more stable than the (0 0 1) surface. Since Fe_5C_2(0 1 0) and (0 0 1) are observed with X-ray-diffraction synchrotron-radiation experiments [76], direct comparison between these two surfaces is informative. It is noted that reaction activation and selectivity is related with surface structure. It is important for investigating the F–T reactions on stable Fe_5C_2(0 1 0) and active (0 0 1) to understand the whole F–T mechanism. As given in Table 6, C + CO → CCO coupling has high barrier (2.04 eV [77]) and is endothermic (0.81 eV [78]) on (0 1 0)(0.25), but it has low barrier (0.66 eV) and is thermal neutral (0.01 eV) on (0 0 1)(0.0). This suggests CCO formation is more favored on Fe_5C_2(0 0 1) than on Fe_5C_2(0 1 0).

For other iron carbide, C + CO → CCO on the most stable Fe_2C(0 1 1), Fe_3C(0 0 1), and Fe_4C(1 0 0) has barrier of 0.93, 1.89, and 0.64 eV, respectively, and is endothermic by 0.87, 1.05, and 0.62 eV, respectively [77]. This indicates that CCO formation is not favored on the most stable Fe_5C_2(0 1 0), Fe_2C(0 1 1), Fe_3C(0 0 1), Fe_4C(1 0 0), while CCO formation is favored on the less stable Fe_5C_2(0 0 1). For Fe_3C, (1 0 0) is much less stable than (0 0 1) surface [79], this reaction on Fe_3C(1 0 0) is thermal neutral (0.02 eV) [80]. Thus, CCO formation on Fe_3C(1 0 0) is also favored. This indicates that chain initiation mechanism on more stable FeC_x surfaces and less stable FeC_x surfaces might be different. On active Fe_5C_2(0 0 1), the chain initiation is CO insertion with CCO formation (insertion mechanism), while on the most stable Fe_5C_2(0 1 0), CO is preferred to hydrogenation to form CH_x [77] (carbide mechanism). Thus, Fe_5C_2(0 1 0) and (0 0 1) provide the basis for understanding their differences in FTS mechanism.

Compared to the perfect surface, the adsorption energy and dissociation barrier of CO at defect site of Fe_5C_2(0 0 1) is larger and lower, respectively; as also found on the defect Fe_2C(0 1 1), Fe_5C_2(0 1 0), Fe_3C(0 0 1), Fe_4C(1 0 0) [77], and Fe_3C(1 0 0) surfaces [40]. Therefore, defect sites will help CO adsorption and dissociation. On Fe_5C_2(0 0 1), CO hydrogenation barriers at defect site and perfect surface are lower than the dissociation barriers; and this suggests that hydrogenation of CO promotes C–O cleavage via formyl (CHO) intermediate. Indeed, King et al. studied the mechanism of hydrocarbon combustion and synthesis on Pd(1 1 1), Pt(1 1 1), and Ru(0 0 0 1) surfaces, and confirmed formyl is main intermediate species in both processes [81]. The emerging of defect sites during the process of surface C hydrogenation and coupling play important role for regenerating the active site and sustaining the catalytic cycle.

In the process of FTS, CO at vacancy site is more preferred to adsorption, activation, hydrogenation and dissociation compared with perfect Fe_5C_2(0 0 1). Thus, CO filling at vacancy site promotes CH species formation and increases the coverage of O atoms. On the other hand, O hydrogenation into H_2O is favored at the high coverage of O. Therefore, CO filling at vacancy site and H_2O formation and removal both promote the regeneration of the active site and sustain the catalytic cycle.

4. Conclusion

The chain growth mechanism of FTS on Fe_5C_2(0 0 1) were investigated at the levels of density functional theory by using CASTEP programs. The carbide mechanism and CO insertion mechanism were considered.

For co-adsorbed H, CO and surface carbon atoms, the formation of CH and CCO is most favored in the first steps of FTS; and CO is the chain initiator. Since CH + CCO has high barrier, CH dehydrogenation and then coupling with CCO to form CCCO is more favored. Compared with CCO coupling, CCO hydrogenation to form CCH_2 and CHCH is also favored.

For CCH_2 hydrogenation, dehydrogenation and coupling with CH, CO and C atoms, CCH_2 dehydrogenates into CCH at first, and then couple with C to form CCCH. CHCH also dehydrogenates into CCH at first and then couple with C to form CCCH. Therefore, CCO and CCH are the main C_2 species, and CCCO and CCCH are the main C_3 intermediates.

For chain propagation from C_2 to C_3, C atom is the most favored C_1 species. Since chain initiation obeys CO insert mechanism and chain propagation obeys carbide mechanism, both mechanisms do work synergistically rather than independently.

It is found that the vacancy sites formed from surface carbon hydrogenation and the subsequent coupling reactions can be dynamically filled by CO activation, promoted by subsequent hydrogenation into surface formyl intermediate (CHO) and successive dissociation into surface CH and O. Apart from surface CH hydrogenation into hydrocarbons, surface O hydrogenation into water is also very important for generating and maintaining the surface stability and reactivity. It is found that surface O hydrogenation into surface OH is favored at high coverage. H_2O formation

from surface OH disproponation is energetically more favored than surface OH hydrogenation.

Acknowledgments

This work was supported by Chinese Academy of Science and the National Nature Foundation of China (No. 20873173) and National Basic Research Program of China (No. 2011CB201406). This work was also supported by Synfuels China Co., Ltd.

Appendix A. Supplementary data

The energy barriers and reaction energies without ZPEC of each reaction is given.

Supplementary data associated with this article can be found, in the online version, at doi:10.1016/j.molcata.2011.06.009.

References

[1] R.B. Anderson, The Fischer–Tropsch Reaction, Academic Press, London, U.K., 1984.
[2] S. Li, R.J. O'Brien, G.D. Meitzner, H. Hamdeh, B.H. Davis, E. Iglesia, Appl. Catal. A 219 (2001) 215.
[3] A.K. Datye, Y.M. Jin, L. Mansker, R.T. Motjope, T.H. Dlamini, N.J. Coville, Stud. Surf. Sci. Catal. 130B (2000) 1139.
[4] C.H. Bartholomew, M.W. Stoker, L. Mansker, A.K. Datye, Stud. Surf. Sci. Catal. 126 (1999) 265.
[5] Y. Yang, H.-W. Xiang, Y.-Y. Xu, L. Bai, Y.-W. Li, Appl. Catal. A 266 (2004) 181.
[6] Y. Yang, H.-W. Xiang, L. Tian, H. Wang, C.-H. Zhang, Z.-C. Tao, Y.-Y. Xu, B. Zhong, Y.-W. Li, Appl. Catal. A 284 (2005) 105.
[7] M. Ding, Y. Yang, J. Xu, Z.-C. Tao, H. Wang, H. Wang, H.-W. Xiang, Y.-W. Li, Appl. Catal. A 345 (2008) 176.
[8] B.H. Davis, Catal. Today 84 (2003) 83.
[9] (a) E. de Smit, M.M. van Schooneveld, F. Cinquini, H. Bluhm, P. Sautet, F.M.F. de Groot, B.M. Weckhuysen, Angew. Chem. Int. Ed. 50 (2011) 1584;
(b) E. de Smit, F. Cinquini, A.M. Beale, O.V. Safonova, W. van Beek, P. Sautet, B.M. Weckhuysen, J. Am. Chem. Soc. 132 (2010) 14928.
[10] M.E. Dry, Hydrocarb. Process. 61 (1982) 121.
[11] J.J.C. Geerlings, J.H. Wilson, G.J. Kramer, H.P.C.E. Kuipers, A. Hoek, H.M. Huisman, Appl. Catal. A 186 (1999) 27.
[12] M.E. Dry, Catal. Today 71 (2002) 227.
[13] (a) F. Fischer, H. Tropsch, Brennstroff-Chem. 7 (1926) 97;
(b) F. Fischer, H. Tropsch, Chem. Ber. 59 (1926) 830.
[14] R.C. Brady III, R. Pettit, J. Phys. Chem. 91 (1987) 929.
[15] P.J.R. Biloen, Neth. Chem. Soc. 99 (1980) 33.
[16] P. Biloen, W.M.H. Sachtler, Adv. Catal. 30 (1981) 165.
[17] P. Biloen, J.N. Helle, W.M.H. Sachtler, J. Catal. 58 (1979) 95.
[18] C.A. Mims, L.E. McCandlish, M.T. Melchior, Catal. Lett. 1 (1988) 121.
[19] F. Ma, G.J. Sunley, I.M. Saez, P.M. Maitlis, J. Chem. Soc., Chem. Commun. (1990) 1279.
[20] M.L. Turner, P.K. Byers, H.C. Long, P.M. Maitlis, J. Am. Chem. Soc. 115 (1993) 4417.
[21] M.L. Turner, H.C. Long, A. Shenton, P.K. Byers, P.M. Maitlis, Chem. Eur. J. 1 (1995) 549.
[22] P.M. Maitlis, H.C. Long, R. Quyoum, M.L. Turner, Z.-Q. Wang, J. Chem. Soc., Chem. Commun. (1996) 1.
[23] H.C. Long, M.L. Turner, P. Fornasiero, J. Kaspar, M. Graziani, P.M. Maitlis, J. Catal. 167 (1997) 172.
[24] P.M. Maitlis, R. Quyoum, H.C. Long, M.L. Turner, Appl. Catal. A 186 (1999) 363.
[25] B.E. Mann, M.L. Turner, R. Quyoum, N. Marsih, P.M. Maitlis, J. Am. Chem. Soc. 121 (1999) 6497.
[26] D.S. Jordan, A.T. Bell, J. Phys. Chem. 90 (1986) 4797.
[27] F.A.P. Cavalcanti, R. Oukaci, I. Wender, D.G. Blackmond, J. Catal. 123 (1990) 270.
[28] R. Snel, R.L. Espinoza, J. Mol. Catal. A 43 (1987) 237.
[29] J.H. Boelee, J.M.G. Cuesters, K. van der Wiele, Appl. Catal. 53 (1989) 1.
[30] A.A. Adesina, R.R. Hudgins, P.L. Silveston, Appl. Catal. 62 (1990) 295.
[31] L.M. Tau, H.A. Dabbagh, B. Chwala, B.H. Davis, Catal. Lett. 7 (1990) 141.
[32] E. Iglesia, S.C. Reyes, R.J. Madon, S.L. Soled, Adv. Catal. 39 (1993) 221.
[33] I.M. Ciobica, F. Frechard, R.A. van Santen, A.W. Kleyn, J. Hafner, Chem. Phys. Lett. 311 (1999) 185.
[34] I.M. Ciobica, F. Frechard, R.A. van Santen, A.W. Kleyn, J. Hafner, J. Phys. Chem. B 104 (2000) 3364.
[35] I.M. Ciobica, G.J. Kramer, Q. Ge, M. Neurock, R.A. van Santen, J. Catal. 212 (2002) 136.
[36] Z.-P. Liu, P. Hu, J. Am. Chem. Soc. 224 (2002) 11568.
[37] J. Chen, Z.-P. Liu, J. Am. Chem. Soc. 130 (2008) 7929.
[38] J.M.H. Lo, T. Ziegler, J. Phys. Chem. C 111 (2007) 13149.
[39] J.M.H. Lo, T. Ziegler, J. Phys. Chem. C 112 (2008) 13681.
[40] L.-J. Deng, C.-F. Huo, X.-W. Liu, X.-H. Zhao, Y.-W. Li, J. Wang, H. Jiao, J. Phys. Chem. C 114 (2010) 21585.
[41] C.K. Rofer-DePoorter, Chem. Rev. 81 (1981) 447.
[42] H. Pichler, H. Schulz, Chem. Ind. Technol. 42 (1970) 1162.
[43] J.T. Kummer, H. Podgurski, W.B. Spencer, P.H. Emmett, J. Am. Chem. Soc. 73 (1951) 564.
[44] J.T. Kummer, P.H. Emmett, J. Am. Chem. Soc. 75 (1953) 5177.
[45] J. Cheng, P. Hu, P. Ellis, S. French, G. Kelly, C. Martin Lok, J. Phys. Chem. C 112 (2008) 9464.
[46] O.R. Inderwildi, S.J. Jenkins, D.A. King, J. Phys. Chem. C 112 (2008) 1305.
[47] D.-B. Cao, S.-G. Wang, Y.-W. Li, J. Wang, H. Jiao, J. Mol. Catal. A 272 (2007) 275.
[48] K.J. Smith, R.B. Anderson, J. Catal. 85 (1984) 428.
[49] Y.T. Eidus, Russ. Chem. Rev. (Engl. Tranl.) 36 (1967) 338.
[50] R.J. Klingler, J.C. Huffman, J.K. Kochi, Inorg. Chem. 20 (1981) 34.
[51] C.P. Casey, C.J. Czerwinski, R.K. Hayashi, J. Am. Chem. Soc. 117 (1995) 4189.
[52] W.S. Ning, N. Koizumi, H. Chang, T. Mochizuki, T. Itoh, M. Yamada, Appl. Catal. A 312 (2006) 35.
[53] J.F. Shultz, W.K. Hall, B. Seligman, R.B. Anderson, J. Am. Chem. Soc. 77 (1955) 213.
[54] D.B. Bukur, M. Koranne, X.S. Lang, K.R.P.M. Roa, G.P. Huffman, Appl. Catal. A 126 (1995) 85.
[55] H. Hayakawa, H. Tanaka, K. Fujimoto, Appl. Catal. A 310 (2006) 24.
[56] S.Z. Li, R.J. O'Brien, G.D. Meitzner, H. Hamdeh, B.H. Davis, E. Iglesia, Appl. Catal. A 219 (2001) 215.
[57] A. Michaelides, P. Hu, J. Chem. Phys. 114 (2001) 513.
[58] A. Michaelides, P. Hu, J. Am. Chem. Soc. 123 (2001) 4235.
[59] X.-Q. Gong, R. Raval, P. Hu, Mol. Phys. 102 (2004) 993.
[60] M.C. Payne, D.C. Allan, T.A. Arias, J.D. Joannopoulos, Rev. Mod. Phys. 64 (1992) 1045.
[61] V. Milman, B. Winkler, J.A. White, C.J. Pickard, M.C. Payne, E.V. Akhmataskaya, R.H. Nobes, Int. J. Quantum Chem. 77 (2000) 895.
[62] D. Vanderbilt, Phys. Rev. B 41 (1990) 7892.
[63] J.P. Perdew, K. Burke, M. Ernzerhof, Phys. Rev. Lett. 77 (1996) 3865.
[64] H.J. Monkhorst, J.D. Pack, Phys. Rev. B 13 (1976) 5188.
[65] S.G. Louie, S. Froyen, M.L. Cohen, Phys. Rev. B 26 (1982) 1738.
[66] T.A. Halgren, W.N. Lipscomb, Chem. Phys. Lett. 49 (1977) 225.
[67] D.-B. Cao, Y.-W. Li, J. Wang, H. Jiao, J. Phys. Chem. C 112 (2008) 14883.
[68] M.-L. Bocquet, A. Michaelides, D. Loffreda, P. Sautet, A. Alavi, D.A. King, J. Am. Chem. Soc. 125 (2003) 5620.
[69] D.M. Stockwell, D. Bianchi, C.O. Bennett, J. Catal. 113 (1988) 13.
[70] M. Boudart, G. Djéga-Mariadassou, in: Kinetics of Heterogeneous Catalytic Reactions, Princeton Univ.; V.P. Zhdanov, J. Pavlicek, Z. Knor, Catal. Rev. Sci. Eng. 30 (1988) 501.
[71] Z. Tao, Y. Yang, M. Ding, T. Li, H. Xiang, Y.-W. Li, Catal. Lett. 117 (2007) 130.
[72] Y. Chen, G.V. Dionisios, J. Phys. Chem. C114 (2010) 4973.
[73] D.-B. Cao, F.-Q. Zhang, Y.-W. Li, H. Jiao, J. Phys. Chem. B 108 (2004) 9094.
[74] X.-Q. Gong, R. Raval, P. Hu, Surf. Sci. 562 (2004) 247.
[75] P.J. Steynberg, J.A. van den Berg, W.J. van Rensburg, J. Phys.: Condens. Matter 20 (2008) 064238.
[76] A. Koniger, C. Hammerl, M. Zeitler, B. Rauschenbach, Phys. Rev. B 55 (1997) 8143.
[77] C.-F. Huo, Y.-W. Li, J. Wang, H. Jiao, J. Am. Chem. Soc. 131 (2009) 14713.
[78] D.C. Sorescu, J. Phys. Chem. C 113 (2009) 9256.
[79] W.C. Chiou Jr., E.A. Carter, Surf. Sci. 530 (2003) 87.
[80] X.-Y. Liao, D.-B. Cao, S.-G. Wang, Z.-Y. Ma, Y.-W. Li, J. Wang, H. Jiao, J. Mol. Catal. A 269 (2007) 169.
[81] O.R. Inderwildi, S.J. Jenkins, D.A. King, Angew. Chem. Int. Ed. 47 (2008) 5253.